GeoScienceWorld
Lithosphere
Volume 2022, Article ID 5446117, 28 pages
https://doi.org/10.2113/2022/5446117

Lithosphere

*Research Article*

# Origin and Characteristics of the Crude Oils and Condensates in the Callovian-Oxfordian Carbonate Reservoirs of the Amu Darya Right Bank Block, Turkmenistan

**Yunpeng Shan**,[1,2] **Hui Chai**,[3] **Hongjun Wang**,[1,2,4] **Liangjie Zhang**,[1] **Penghui Su**,[1,4] **Xiangwen Kong**,[1,2] **Zhenhua Bai**,[1,2] **Muwei Cheng**,[1] **and Hongwei Zhang**[1]

[1]*PetroChina Research Institute of Petroleum Exploration and Development, Beijing 100083, China*
[2]*Key Laboratory of Petroleum Geochemistry of PetroChina, Beijing 100083, China*
[3]*China National Oil and Gas Exploration and Development Company Ltd., Beijing 100034, China*
[4]*State Key Laboratory of Enhanced Oil Recovery, Beijing 100083, China*

Correspondence should be addressed to Yunpeng Shan; shan_yunpeng@petrochina.com.cn

Received 29 October 2021; Revised 15 September 2022; Accepted 29 September 2022; Published 18 October 2022

Academic Editor: Songjian Ao



The Amu Darya Right Bank Block is located northeast of the Amu Darya basin, a large petroliferous sedimentary basin, with abundant natural gas resources in carbonate rocks under the ultra-thick gypsum-salt layer. Oil fields producing crude oils have recently been found around large gas fields. Unraveling the origins of the crude oils is crucial for effective petroleum exploration and exploitation. The origin of gas condensates and crude oils was unraveled through the use of comprehensively analytical and interpretative geochemical approaches. Based on oil-source correlation, the reservoir forming process has been restored. The bulk geochemical parameters of the local source rocks of the ADRBB indicated that the local sources have hydrocarbon generation and accumulation potential. The middle-lower Jurassic coal-bearing mudstone is gas prone, while the mudstone of the Callovian-Oxfordian gap layer is oil prone, and the organic matter type of Callovian-Oxfordian carbonate rocks is the mixed type between the two previous source rocks. The interpretation schemes for compositions of n-alkanes, pristane and phytane, $C_{27}$–$C_{28}$–$C_{29}$ sterane distributions, $C_{19}$+$C_{20}$–$C_{21}$–$C_{23}$ tricyclic terpane distributions, extended tricyclic terpane ratio, and $\delta^{13}C$ indicated that crude oil is likely from marine organic matter, while condensates mainly originate from terrestrial organic matter. However, from the perspective of the 18$\alpha$-trisnorneohopane/17$\alpha$-trisnorhopane and isomerization ratio of $C_{29}$ sterane, condensates are too mature to have originated in the local source rocks of the ADRBB, whose maturity is well comparable with that of crude oils. The geochemical, geologic, and tectonic evolutions collectively indicate that the crude oils were most likely generated and migrated from the relatively shallow, lowly mature gap layer and Callovian-Oxfordian carbonate rocks of the ADRBB, while the condensates mostly originated from the relatively deep and highly mature middle-lower coal-bearing mudstone and Callovian-Oxfordian carbonate rocks in the Murgab depression in the southeast of the basin. Basement faults are the key factors affecting the types of oil and gas reservoirs. During the periods of oil and gas migration, traps with basement faults mainly captured natural gas and condensates and traps without basement faults were enriched with crude oils generated from local source rocks.

## 1. Introduction

The Amu Darya Right Bank Block (ADRBB) covers approximately $1.86 \times 10^4$ km$^2$ and is located northeast of the Amu Darya basin, a large hydrocarbon-rich depositional basin on the southeastern Turan platform (Figures 1 and 2). The Callovian-Oxfordian carbonate reservoirs in the ADRBB are the major reservoirs for natural gas and condensate accumulation [1]. However, since 2020, the Wes-2 well, located in the middle section of the ADRBB, has begun producing crude oils [2]. The appearance of crude oils indicates that the formation process of hydrocarbon reservoirs in the

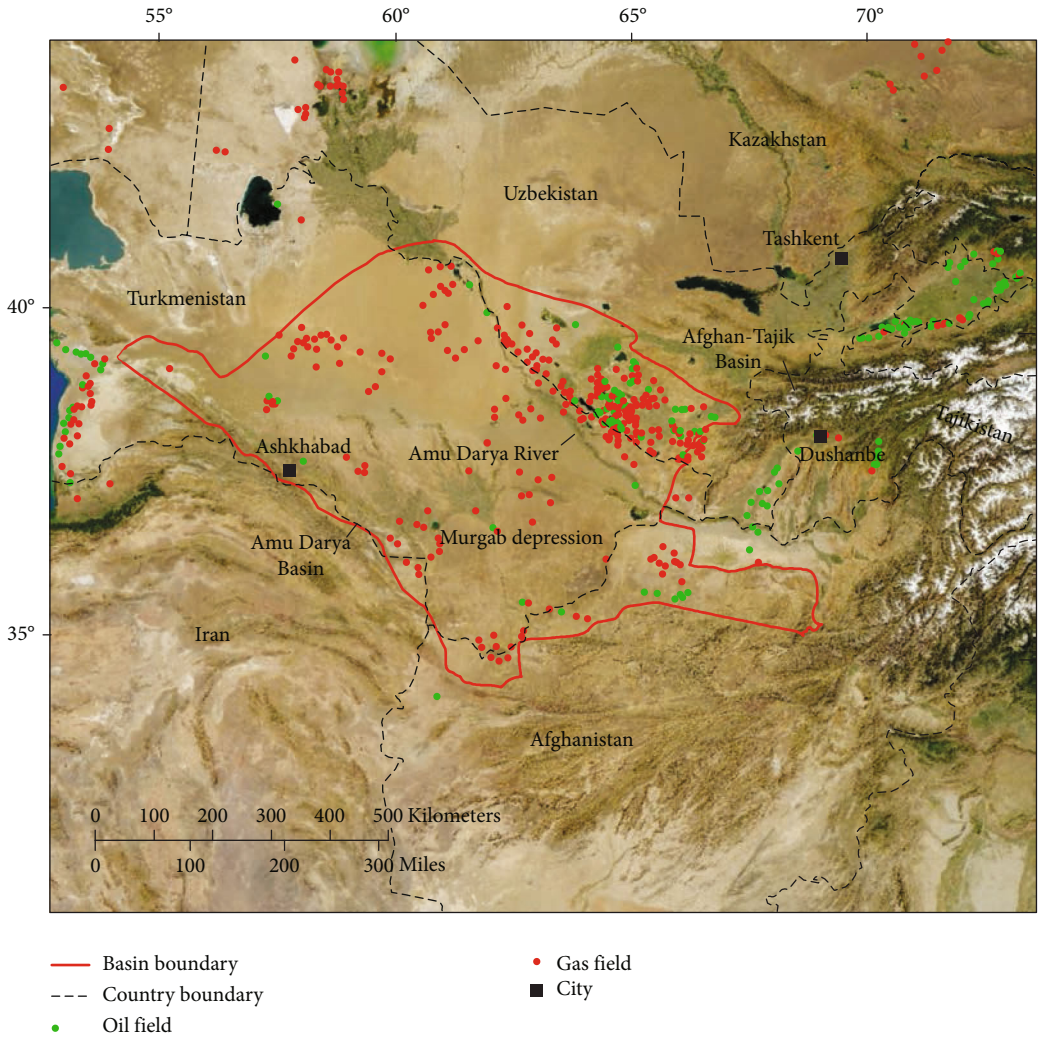


Figure 1: Geological map of the Amu Darya basin (modified from the U.S. Geological Survey [68]).

ADRBB is different, and further geochemical investigations are needed to confirm the parent materials of crude oil, natural gas, and condensate. Predecessors have done a lot of studies on the geological settings of hydrocarbon reservoirs in the ADRBB [3–6]; only a small number of geochemical studies have been reported, and these geochemical data are mainly used to describe the petrological characteristics of the reservoirs [7–9]. The oil-source correlation cannot be performed, and the hydrocarbon migration pathways cannot be described in geochemistry due to the lack of comprehensive geochemical analysis of hydrocarbon fluids accumulated in the reservoirs and source rocks in the basin.

The primary purpose of this study is to decipher the origin of the condensates and the newly found crude oils in the ADRBB. To achieve this, the geochemical indexes used for oil source correlation in scientific research have been used as thoroughly as possible. The parameters include isoprenoids, n-alkanes, steranes, terpanes, carbon isotope, and slope factor of alkane. The acyclic isoprenoids, pristane (Pr), and phytane (Ph), which occur together in ancient sediments and their oil products, are believed to have been formed from chlorophyll by the thermal evolution process [10]. The ratio of pristane to phytane (Pr/Ph) can usually indicate the redox conditions of the sedimentary environment [11, 12], while the ratio of pristane to $nC_{17}$ and phytane to $nC_{18}$ can distinguish the type, thermal maturity, and biodegradation of sedimentary organic matter and oils [13–15]. Moreover, the values of mole percent n-alkanes can indicate the maturity and biodegradation of oil [16]. The main peak carbon of low-maturity oil is large, usually around $C_{15}$ or even larger. At the same time, the chromatographic curve of the low-maturity oil shows serrated, with the carbon predominance index (CPI) and odd-even predominance (OEP) being deviated from 1. On the contrary, the main peak carbon of high maturity oil is small, commonly $C_5$ or $C_6$. The chromatographic curve is relatively smooth, with the CPI and OEP close to 1 [17–22]. Furthermore, the baseline bump of the chromatographic curve represents the existence of unresolved complex mixtures (UCM), which are formed by the strong biodegradation of oil in geological history [23–27]. Thompson [28] reported that the hybrid condensates may have an excess of $C_7$

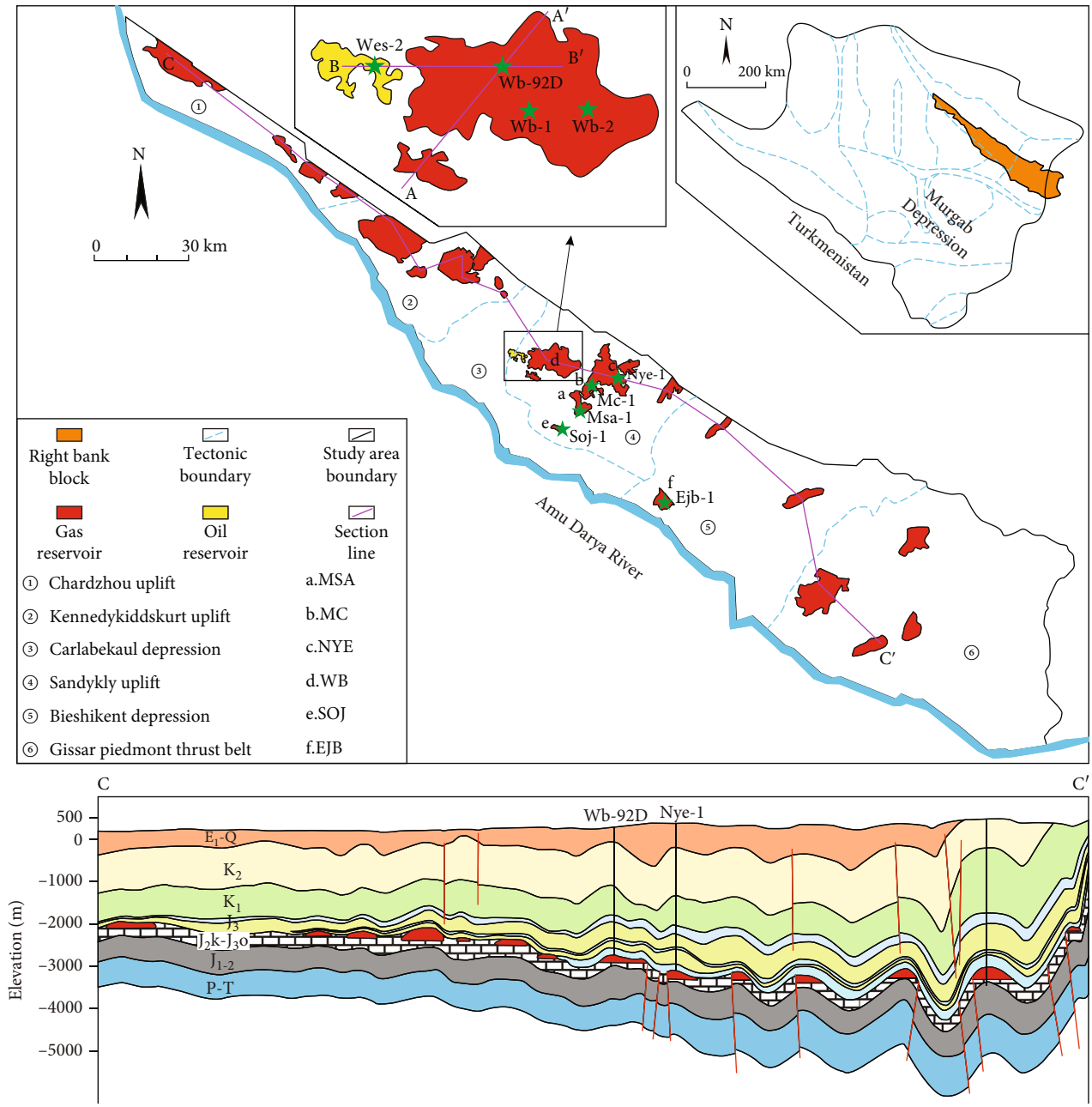


FIGURE 2: Division of structural units and regional cross-section of the ADRBB (modified from Shan et al. [2]).

components, exceeding the projection of the exponential trend established in the $C_{10}$+ region and showing an imperfect exponential regression. In addition, steranes originate from sterols in eukaryotic cell membrane lipid, which occur in algae and higher plants [29, 30]. Tricyclic terpanes originate from prokaryotic cell membranes [31]. It has also been suggested that the enrichment of tricyclic terpanes is related to the input of marine algae [32–35]. The relative proportions of regular steranes [36–41] and tricyclic terpanes [42–47] in living organisms are related to specific environments. It is believed that steranes and tricyclic terpanes in sediments might provide valuable paleoenvironmental information. For some compounds in steranes or terpanes, such as $C_{29}$ regular steranes, 18$\alpha$-trisnorneohopane, and $C_{32}$ hopanes (the latter two are pentacyclic triterpenes), the relative content of thermally stable geological molecular configuration can indicate the maturity of organic matter, which is widely used to indirectly calculate the maturity of oil [14, 47–51]. Gammacerane ($C_{30}H_{52}$) is a special pentacyclic triterpene with a six-membered ring E, while its isomer, $C_{30}$ hopanes ($C_{30}H_{52}$), which also belong to pentacyclic triterpenes, possesses a five-membered ring E [52]. The gammacerane index, the ratio of gammacerane to $C_{30}$ hopanes, was initially associated with hypersaline paleoenvironments but more recently has been extended and established as marker for water-column stratification [53–57]. In fact, the

essence of water-column stratification is the different water density, which can be affected by salinity, so the gammacerane index that can characterize water-column stratification has a certain relationship with water salinity. From the perspective of elements, stable carbon isotopic is of great importance in the analysis of the oil source since the formation process of oil and gas is the process of kerogen cracking. Kinetic cracking, which preferentially breaks $^{12}C$–$^{12}C$ bonds from kerogen to pyrolysate compared with $^{12}C$–$^{13}C$ bonds and $^{13}C$–$^{13}C$ bonds, could be a plausible explanation of isotopic fractionation in geological history. Therefore, kerogen pyrolysis products from the same source, such as oil, gas, and pyrobitumen, are isotopically comparable, which can provide clues for oil-source correlation [58–62].

The core of the correct interpretation of hydrocarbon migration and accumulation is accurate oil-source correlation which depends on the proper parameter selection. Then, the formation model of hydrocarbon reservoirs can be accurately restored by combining the correlation results with the forming period of hydrocarbon reservoirs and evolution process of traps [2, 63]. The exact reservoir formation model is conducive to identifying and predicting the direction of hydrocarbon migration and accumulation, locating the distribution range of potential and prospective hydrocarbon reservoirs, and guiding the exploration direction, which can provide a highly necessary theoretical support for oil and gas exploration and development.

## 2. Geological Setting

*2.1. Regional Geology.* The Amu Darya basin, which covers an area of 42.7 $km^2$ located in Turkmenistan (65%) and Uzbekistan (25%), extends southwestward into Iran and southeastward into Afghanistan (Figure 1). According to lithology, structural characteristics, and sedimentary period, the Amu Darya basin can be divided into three units upwards: basement, intermediate transition layer, and overlying cover where the petroleum systems are developed [1]. The basement is mainly composed of commonly metamorphosed Paleozoic rocks. The intermediate transition layer consists of Permian-Triassic rocks, which are strongly compacted and diagenetically altered. The overlying cover includes Lower to Middle Jurassic coal-bearing mudstone, Middle to Upper Jurassic carbonates, Upper Jurassic evaporites, Cretaceous-Paleogene marine clastic rocks with carbonate intervals, and Neogene continental clastics [64]. The Amu Darya basin can be divided into some first-order structural units, such as Kopet-Dagh foredeep (southwest of the basin), Murgab depression (southeast of the basin), Khiva-Zaunguz depression (northwest of the basin), and Chardzhou stop (northeast of the basin) based on the morphology of the basement and structural fluctuation [1, 65]. The ADRBB, which is surrounded by the Amu Darya River and the country boundary of Turkmenistan-Uzbekistan-Afghanistan, is located on the southeast of the Chardzhou step (Figure 2). The block is divided into three sections: west, middle, and east, which contain six secondary structural units. The western section is composed of the Chardzhou uplift and Kennedykiddskurt uplift. The middle section includes Carlabekaul depression, Sandykly uplift, and Bieshikent depression. The eastern section consists of the Gissar piedmont thrust belt [66, 67].

*2.2. Stratigraphic Background.* The thick Lower to Middle Jurassic, largely continental, coal-bearing rocks are the main source rocks in the Amu Darya basin (the Lower to Middle Jurassic source rocks are denoted by $J_{1\text{-}2}$ coal-bearing rocks). And the overlying Callovian-Oxfordian carbonates, which are denoted by $J_2k$-$J_3o$, are the major gas-paying beds conformably overlain by thick gypsum-salt rocks of the Gordak Formation, which were deposited on the Kimmeridgian-Tithonian time (Figure 3) [69–73]. The Callovian-Oxfordian carbonates contain a certain proportion of argillaceous limestone with high organic matter content, which is another set of source rocks in the Amu Darya basin [74]. Furthermore, at the end of the Oxfordian period, a set of black mudstones with high gamma values developed in the east-central part of the basin, which is the secondary source rocks in the Amu Darya basin. In the ADRBB, the black mudstone layer, also known as the gap layer, is developed only in the middle-east of the block, with a small thickness, mostly between 5 and 20 m [66, 67]. From bottom to top, the Lower to Middle Jurassic coal-bearing mudstone, the Callovian-Oxfordian carbonates, the gap layer, and the Kimmeridgian-Tithonian gypsum-salt layer form a set of the good reservoir forming assemblage, which provides a material basis for the formation of large gas fields on the ADRBB [75–77].

*2.3. Sedimentary Facies.* The ADRBB has experienced the evolution process of continental-marine-lagoon facies. After being uplifted in the Late Triassic, the ADRBB reentered a subsidence stage in the Early-Middle Jurassic ($J_{1\text{-}2}$). The depositional environment of the ADRBB gradually evolved from delta to marine facies [1, 2, 78, 79]. The ADRBB experienced a large-scale transgression in the Callovian period of the Middle-Late Jurassic ($J_2k$), and a Callovian ramp carbonate platform developed on the basis of the formed accommodation space in this period. During the Oxfordian period ($J_3o$), the ADRBB experienced another transgression. The carbonate platform was generally submerged and retreated and then evolved to a rimmed shelf-type carbonate platform with marginal reefs (Figure 4) [64, 66]. In the Late Jurassic Kimmeridgian period, the ADRBB began to enter the gypsum deposition stage and the carbonate platform gradually degenerated into an evaporitic platform [80]. The ultrathick gypsum-salt layer developed then, widely protecting oil and gas reservoirs.

## 3. Materials and Methods

*3.1. Samples.* Core samples for source rock evaluation and oil correlation were collected from Lower to Middle Jurassic coal-bearing rocks at wells Msa-1, Mc-1, Nye-1, and Wb-1 (3416 m–4130 m; the depth range refers to the range from the shallowest depth to the deepest depth of the wells sampled in this layer, the same as follows). The Callovian-Oxfordian carbonate source rocks were taken wells Msa-1,

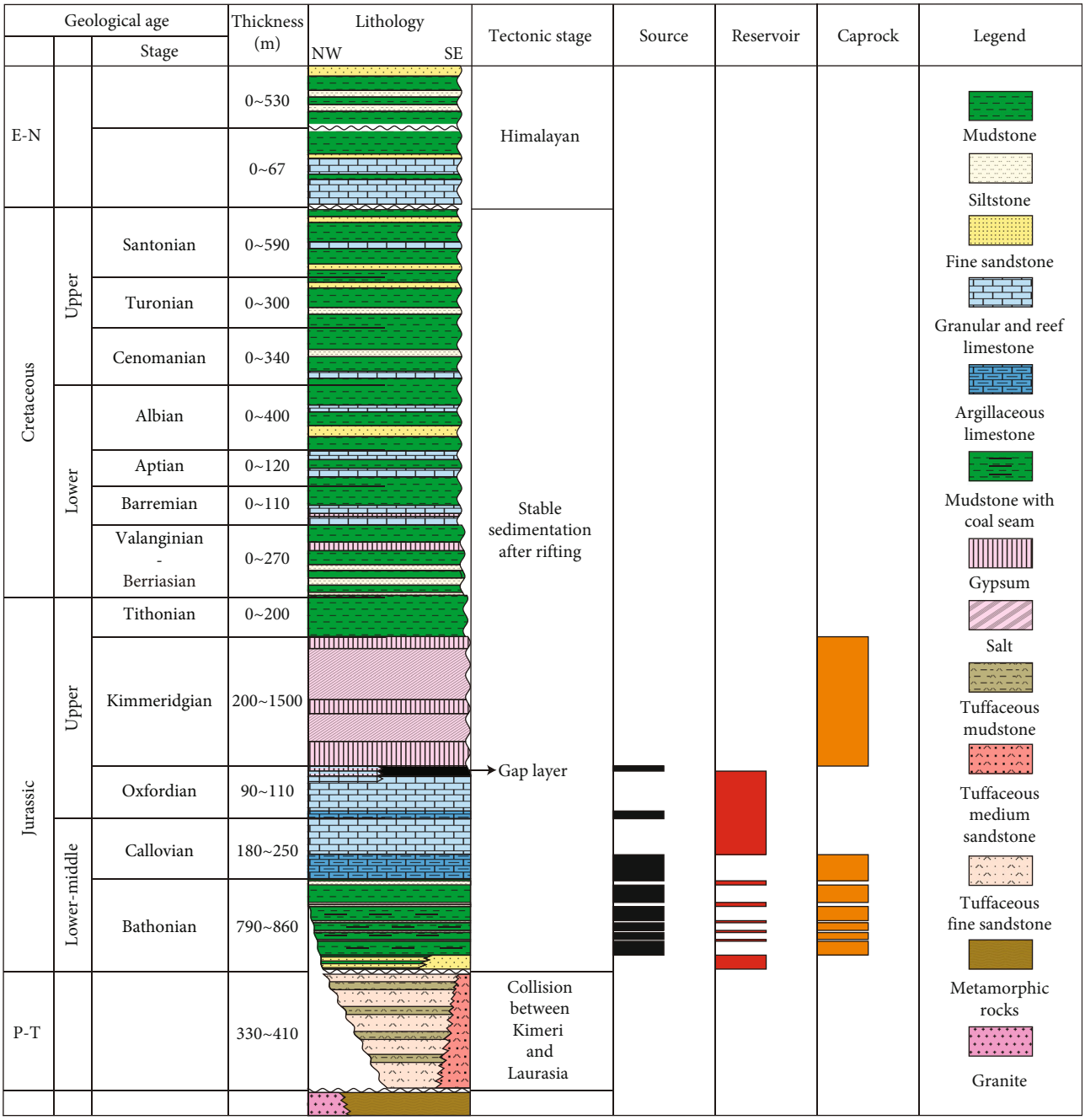


Figure 3: Comprehensive histogram of strata of the ADRBB (modified from Wang et al. [73]).

Sa-2, Mc-1, Soj-1, Nye-1, Wb-1, Wb-16, and Ejb-1 (3170 m–4320 m). The gap source rocks, which only developed in the middle-east of the ADRBB, were collected at wells Msa-1, Mc-1, Nye-1, Wb-1, and Ejb-1 (3026 m–4065 m).

The crude oil and condensate samples were collected from the middle part of the block. The condensate came from well Wb-92D while the crude oil came from well Wes-2. The samples were stored in Schlumberger single-phase-sampling cylinders from the holding tank associated with each well. Crude oil and condensate samples were analyzed immediately after sampling to avoid volatilization of light hydrocarbon and contamination.

### 3.2. Methods

*3.2.1. Source Rock Evaluation.* The total organic carbon content (TOC) of source rocks, which can characterize the organic enrichment, was measured by the LECO CS-230 Carbon/Sulfur analyzer. The Rock-Eval-6 pyrolysis instrument determined the pyrolysis data of source rocks, which can characterize the abundance, type, and maturity of organic matter. The $S_1$ peak of residual hydrocarbon was analyzed at 300°C for 3 min. The $S_2$ peak of newly generated hydrocarbon is analyzed at the temperature range of 300°C–650°C with a heating rate of 25°C/min. Mean vitrinite

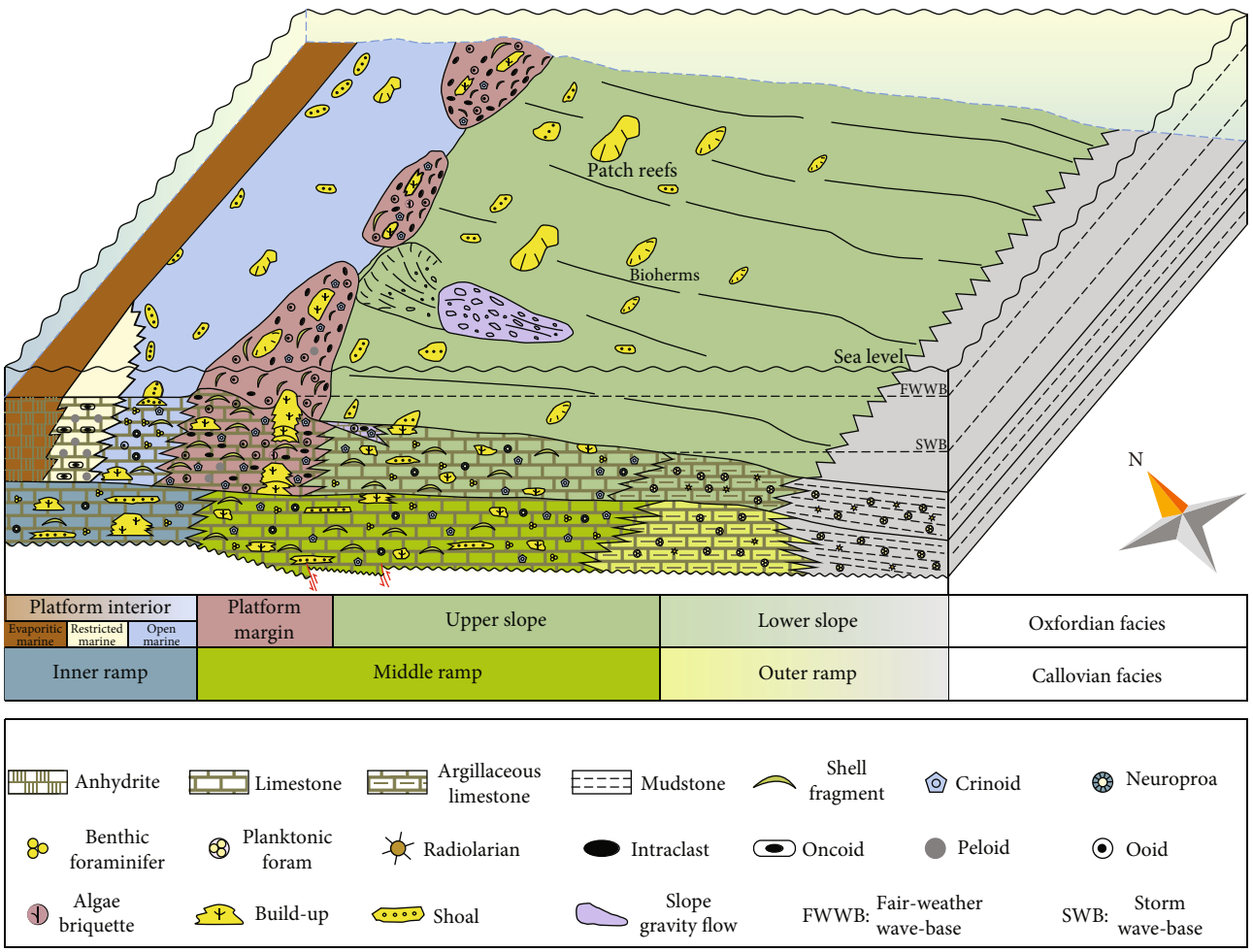


Figure 4: Sedimentary facies of the Oxfordian rimmed carbonate platform of the ADRBB (modified from Li et al. [64]).

reflectance ($R_o$) is based on the measurement of over fifty random-orientation vitrinite particles in each sample to ensure accuracy.

A YSB-automatic multifunction extractor recovered the extractable organic matter (EOM) in source rocks. The EOM solution was evaporated using rotary-evaporation to a small amount for geochemical analysis.

*3.2.2. GC and GC–MS Molecular Characterization.* Bulk molecular characterization for whole oils and EOMs was performed using gas chromatography (GC) methods. Biomarkers of aliphatic, aromatic, and N–S–O compounds in whole oils and EOMs were determined using the gas chromatography–mass spectrum (GC–MS). Before GC–MS analysis, the whole oil and EOMs were complexated to improve the signal-to-noise ratio of the biomarkers. Gas chromatography with flame ionization detector (GC–FID) was equipped with an elastic quartz capillary column DB-5 with a length of 30 m and an inner diameter of 0.25 mm, and the carrier gas was He at a constant flow of 1.0 mL/min. The oven temperature was programmed from 80°C to 310°C, with a 6°C/min heating rate. The GC–MS test runs were based on a Trace GC Ultra system coupled to a dual-stage quadrupole mass spectrometer. The GC was equipped with a programmed temperature vaporizer (PTV) injection system and a DB-5MSUI elastic quartz capillary column (60 m × 0.25 mm × 0.25 mm), and the flow of carrier gas (He) was at a constant rate of 1.0 mL/min. The GC oven was programmed as follows: hold 100°C for 5 min, heating to 220°C at a rate of 4°C/min, then, continue to rise to 320°C at a rate of 2°C/min, and finally, hold at 320°C for 20 min. The mass spectrometer was operated in both full-scan and selected ion monitoring (SIM) modes with an ionization energy of 70 eV.

*3.2.3. Stable Carbon Isotope Analysis.* A Thermo Delta V isotope-ratio mass spectrometer (IRMS) was used to analyze stable carbon isotopes for the source rocks, condensate, and crude oil samples. Solid samples such as kerogen passed through a dynamic rapid combustion module composed of $Cr_2O_3$-Cu-$Ag_2Co_3O_4$ at 1100°C, while liquid samples such as condensates passed through a high-temperature pyrolysis module to completely convert C, H, N, and other atoms into oxides. First, the gas is passed through a water removal trap composed of $Mg(ClO_4)_2$ and then through a 0.5–1 m long GC column to remove $N_2$. The $CO_2$ which removes $H_2O$ and $N_2$ was carried into the IRMS by He for carbon isotope analysis. The carrier gas (He) was at a 300 mL/min constant

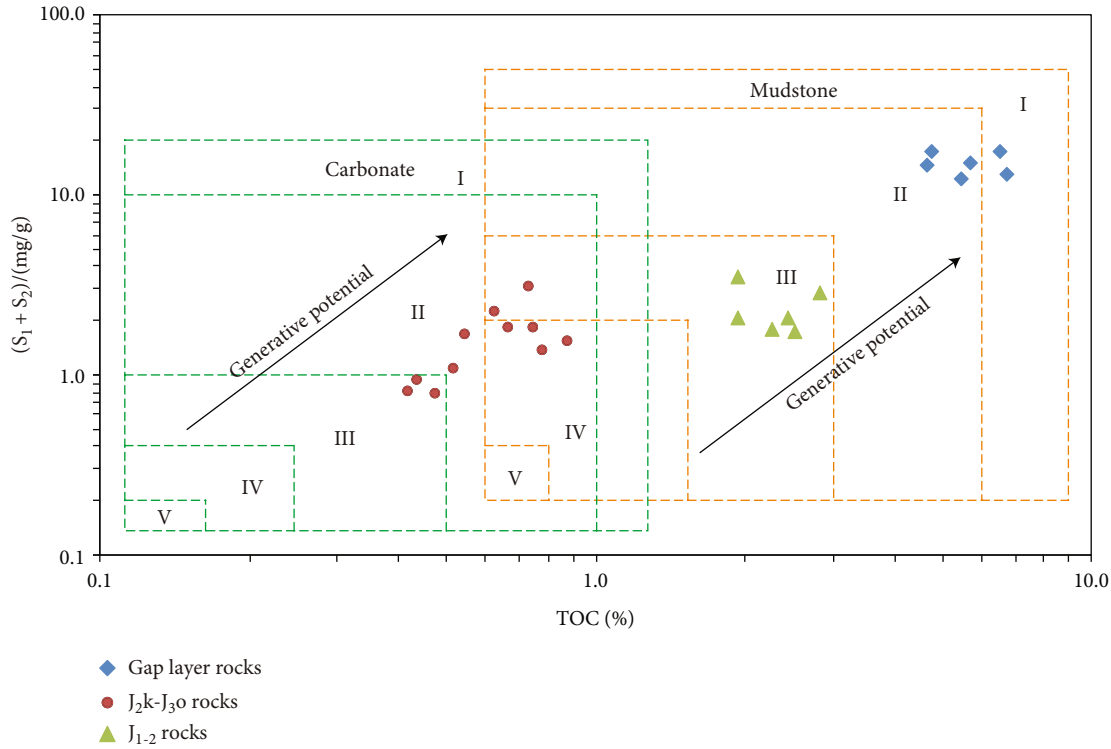


Figure 5: Hydrocarbon generation potential diagram of source rocks (green dashed line for carbonate; orange dashed line for mudstone) (modified from Waples, El Nady et al., and Wang et al. [86–88]).

flow. The $\delta^{13}C$ is calculated according to following the equation [81]:

$$\delta^{13}C = \frac{\left(^{13}C/^{12}C\right)_{\text{Sam}} - \left(^{13}C/^{12}C\right)_{\text{Std}}}{\left(^{13}C/^{12}C\right)_{\text{Std}}} \times 1000‰, \quad (1)$$

which is relative to the Pee Dee Belemnite (PDB) standard. All measurements were performed with relative standard deviations of less than 0.5‰.

*3.2.4. Tectonic Evolution.* The interpreted 3D seismic volume was acquired from the China National Petroleum Corp.; the profiles discussed in this paper were extracted from those 3D seismic data. The data undergo correction, stacking, inverse filtering, migration, and imaging processes. Landmark seismic interpretation system provided the propriety migrated profiles and Society of Exploration Geophysicists (SGY) format files. The software was used to visualize the SGY files and convert vertical time axes to depth. Several drill holes, such as wells Wb-92D, Wes-2, and Wb-1, allow a direct correlation to be made between the seismic and geological units. Balancing and restoration of seismic sections were conducted by stripping off (back-stripping) each sequence and restoring faults and folds by using MOVE® 2016.1 software so that the paleotopography or specific period surfaces were restored to continuous layers with topography [82]. Faults were restored by using the incline-shear algorithm, which assumes that the hanging wall deforms by simple shear and that the footwall remains undeformed by compression. Next, the cross-section was restored by using the flexural-slip unfolding algorithm. After unfolding, the new sequence was backstripped and the same procedure was repeated until only the deepest layer remained.

## 4. Results and Interpretation

*4.1. Bulk Geochemical Parameters of Source Rocks.* The quality of source rocks was evaluated from the organic matter's abundance, type, and maturity. The maturity of source rocks will be discussed in Section 5.2 together with the maturity of crude oils and condensates. Figure 5 is a crossplot of TOC and hydrocarbon generation potential ($S_1 + S_2$) data of source rocks listed in Table 1. Since TOC values and hydrocarbon generation potential values of all samples may differ by up to two orders of magnitude, a double-logarithmic coordinate system is adopted in Figure 5. The TOC percentage varies between 1.93% and 2.84% (average 2.32%) in $J_{1-2}$ coal-bearing mudstone, and that of gap layer mudstone is higher than $J_{1-2}$ coal-bearing mudstone with the range 4.65%–6.73% (average 5.63%). The TOC percentage of $J_2k$-$J_3o$ carbonate ranges from 0.42% to 0.88% (average 0.62%). Similar to TOC percentage, the hydrocarbon generation potential of mudstone source rocks is higher than that of carbonate rocks. The hydrocarbon generation potential of $J_{1-2}$ coal-bearing mudstone varies between 1.72 and 3.51 mg/g (average 2.34 mg/g), and those of gap layer mudstone and $J_2k$-$J_3o$ carbonate are 12.11–17.36 mg/g (average 14.99 mg/g) and 0.77–2.19 mg/g, respectively. According to Peters' [83] and Jarvie's [84] theories, the evaluation criteria

Table 1: Pyrolysis data and atomic ratio data of source rocks.

| Horizon | Well | Depth (m) | TOC (%) | $S_1+S_2$ (mg/g) | O/C | H/C |
|---|---|---|---|---|---|---|
| Gap layer | Msa-1 | 3690 | 6.52 | 17.36 | 0.13 | 1.47 |
| | Mc-1 | 3455 | 4.77 | 17.31 | 0.19 | 1.31 |
| | Mc-1 | 3466 | 5.66 | 15.19 | 0.17 | 1.37 |
| | Nye-1 | 3498 | 4.65 | 14.82 | 0.16 | 1.42 |
| | Wb-1 | 3026 | 6.73 | 13.13 | 0.12 | 1.38 |
| | Ejb-1 | 4065 | 5.43 | 12.11 | 0.15 | 1.33 |
| $J_2k$-$J_3o$ | Msa-1 | 3948 | 0.63 | 2.19 | 0.25 | 1.02 |
| | Sa-2 | 3550 | 0.67 | 1.81 | 0.28 | 1.06 |
| | Sa-2 | 3792 | 0.42 | 0.79 | 0.24 | 1.15 |
| | Mc-1 | 3670 | 0.74 | 3.02 | 0.17 | 1.09 |
| | Soj-1 | 3800 | 0.52 | 1.07 | 0.24 | 0.72 |
| | Soj-1 | 3940 | 0.48 | 0.77 | 0.14 | 0.82 |
| | Nye-1 | 3560 | 0.75 | 1.81 | 0.29 | 0.77 |
| | Nye-1 | 3720 | 0.55 | 1.62 | 0.21 | 0.88 |
| | Wb-1 | 3170 | 0.79 | 1.32 | 0.13 | 0.94 |
| | Wb-16 | 3180 | 0.44 | 0.92 | 0.16 | 0.72 |
| | Ejb-1 | 4320 | 0.88 | 1.48 | 0.31 | 0.91 |
| $J_{1\text{-}2}$ | Msa-1 | 3970 | 1.94 | 3.51 | 0.14 | 0.58 |
| | Mc-1 | 3728 | 2.84 | 2.82 | 0.08 | 0.43 |
| | Soj-1 | 4130 | 2.27 | 1.81 | 0.25 | 0.81 |
| | Nye-1 | 3800 | 2.52 | 1.72 | 0.11 | 0.58 |
| | Wb-1 | 3416 | 2.43 | 2.08 | 0.18 | 0.71 |
| | Wb-1 | 3502 | 1.93 | 2.07 | 0.23 | 0.61 |

Table 2: Quality evaluation standard of source rocks.

| Level | Description | Mudstone | | Carbonate | |
|---|---|---|---|---|---|
| | | TOC (%) | $S_1+S_2$ (mg/g) | TOC (%) | $S_1+S_2$ (mg/g) |
| I | Excellent | >6.0 | >30 | >1.0 | >10 |
| II | Very good | 3.0–6.0 | 6.0–30 | 0.5–1.0 | 1.0–10 |
| III | Good | 1.5–3.0 | 2.0–6.0 | 0.25–0.5 | 0.4–1.0 |
| IV | Fair | 0.8–1.5 | 0.4–2.0 | 0.15–0.25 | 0.2–0.4 |
| V | Poor | <0.8 | <0.4 | <0.15 | <0.2 |

of mudstone and carbonate source rocks are listed in Table 2 and plotted in Figure 5. The zone framed by the orange dashed line in Figure 5 is suitable for evaluating the hydrocarbon generation capacity of mudstones such as $J_{1\text{-}2}$ coal-bearing mudstone and gap layer mudstone, while the zone framed by the green dashed line is adopted to evaluate that of carbonate rocks such as $J_2k$-$J_3o$ carbonate. TOC is generally linearly and positively correlated with hydrocarbon generation potential, so the level of source rocks can be determined by the higher one of the two parameters when they are not in the same level. The $J_{1\text{-}2}$ coal-bearing mudstone belongs to level III (good), while the $J_2k$-$J_3o$ carbonate and the gap layer belong to levels II–III (very good-good) and levels I–II (excellent-very good), respectively. In other words, the hydrocarbon generation capacities of the three sets of source rocks display a general upward increasing trend with the increase in organic matter abundance.

The source rocks corresponding to the initial definition of kerogen types I–III are ranged in the order of decreasing petroleum potential and thus of the H/C ratio [85]. Generally, the atomic H/C ratio of kerogen type I is higher than 1.5 and that of kerogen type III is lower than 0.8. The average atomic H/C ratios of the kerogens of the $J_{1\text{-}2}$ coal-bearing mudstone, the $J_2k$-$J_3o$ carbonate, and the gap layer mudstone are 0.43–0.81 (average 0.62), 0.72–1.15 (average 0.92), and 1.33–1.47 (average 1.38), respectively (Table 1). In the Van Krevelen diagram (Figure 6) using the element ratio parameters of kerogen in Table 1, the kerogens of source rocks upwards are divided into type III, mixed type II/III, and type II. Moreover, three carbonate samples are

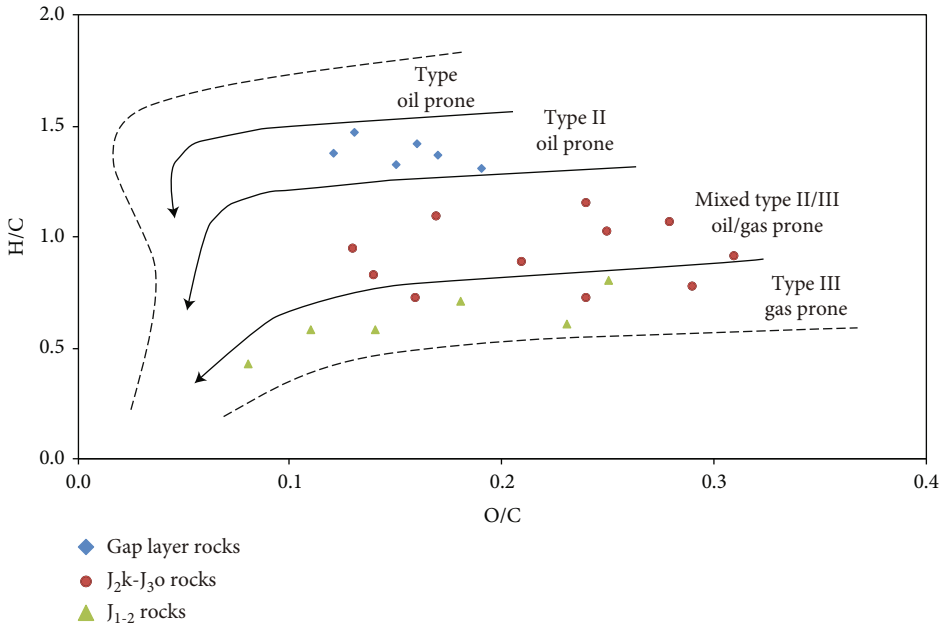


Figure 6: Organic matter types of source rocks (modified from Vandenbroucke and Largeau, Tissot and Welte, and Huang et al. [85, 89, 90]).

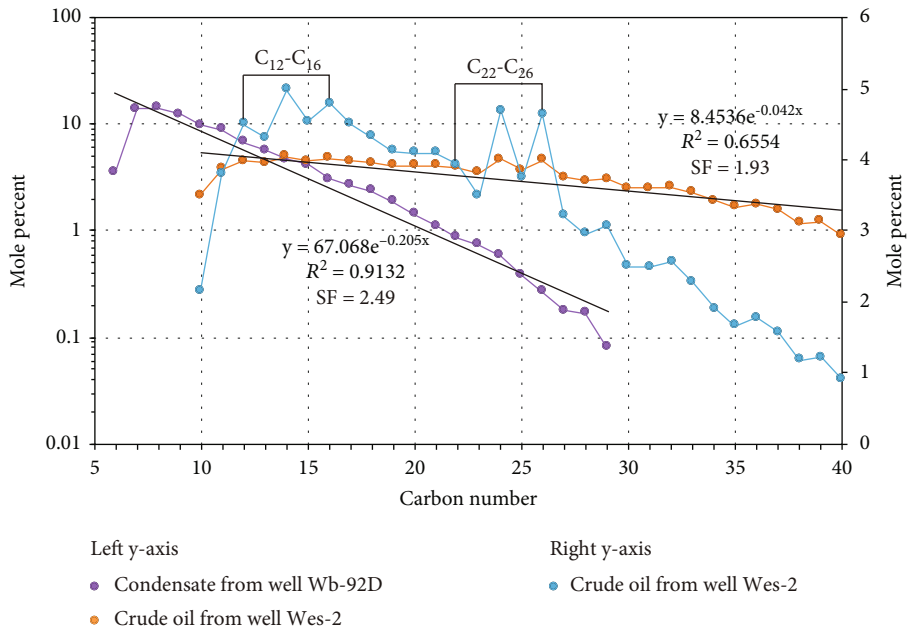


Figure 7: Alkane distribution of the condensates and crude oils.

plotted in the area of type III kerogen, showing that although the sedimentary environment of $J_2k$-$J_3o$ carbonate in the ADRBB is marine facies, and there is still some input of terrestrial organic matter in the process of deposition. These organic matter abundance and kerogen types can serve as liquid petroleum and gas sources.

*4.2. Alkane Distribution Characteristics of Condensates and Crude Oils.* Figure 7 shows plots of mole% alkanes ($y$) versus carbon number ($x$) in log-linear axes for the condensate from well Wb-92D and crude oil from well Wes-2 and linear-linear for the crude oil from well Wes-2. The condensate from well Wb-92D ranges from $C_6$ to $C_{29}$. The $C_{6+}$ components in the condensate from well Wb-92D present an exponential trend ($y = A\,e^{-\alpha x}$) and high slope factor ($SF = e^{\alpha}$), indicating thermogenic origins and negligible alterations. However, the exponential progression's correlation coefficient ($R^2 = 0.913$) is relatively lower than 0.99, indicating that the condensates are formed by a mixing source [13, 28]. The admixture of two petroleum fluids

possessing different but perfect exponential progressions among their components results in a nonexponential product. And the concentration of $C_7$ exceeds $C_6$, which also indicates that it is formed by a mixed source or evaporative fractionation. However, the evaporative fractionation generally leads to a minor exceeding [28]. The significantly exceeding indicates that evaporation fractionation has a limited effect on the condensate formation from well Wb-92D.

The *x*-axis value of each point represents the sum of normal and branched alkanes with this carbon number. The *y* -axis on the left is a logarithmic coordinate used for exponential regression of the mole percentage of condensates and crude oils. The *y*-axis on the right is a linear coordinate used to observe the predominance of even C-numbers in crude oils (modified from Thompson [28]).

The crude oil from well Wes-2 ranges from $C_{10}$ to $C_{40}$. Although the main peak carbon is $C_{14}$, with the content of 4.98%, there is a minor difference between the content of other carbon numbers and that of $C_{14}$, resulting in a low exponential regression correlation coefficient (Figure 7). The evolution process of oil is perceived as a series of increasing from $C_{40}$ to $C_{10}$ in view of the thermal origin, the conversion of heavier to lighter molecules. However, there is a predominance of even C-numbers in $C_{12}$–$C_{16}$ and $C_{22}$–$C_{26}$ with OEP = 0.9 (odd-even predominance), making the curve show a sawtooth shape in the rectangular coordinate system (Figure 7) and indicating that the crude oil from well Wes-2 is in a low-maturity state. The predominance of even C-numbers in $C_{12}$–$C_{16}$ may be attributed to rocky coals with the presence of unsaturated fatty acids and specific inputs from organisms, such as bacteria and diatoms [91–94], while the predominance of even C-numbers in $C_{22}$–$C_{26}$ may relate to reductive processes in highly saline, carbonate environments that were generated from the remains of algal communities [95]. The wide carbon number range, predominance of even C-numbers, and no obvious main peak carbon number imply that the crude oil from well Wes-2 is not the product of single-source rock but mixed and low-maturity source origin.

*4.3. Organic Geochemistry.* Representative steranes and terpane distributions in the condensates and the crude oils from the ADRBB are illustrated using the *m*/*z* 217 and *m*/*z* 191 mass chromatograms in Figure 8. The baselines of the gas chromatograms are relatively flat without the unresolved complex mixture (UCM) hump, indicating that neither condensates nor crude oils have undergone strong biodegradation. The condensate from well Wb-92D has more abundant 5$\alpha$(H),14$\alpha$(H),17$\alpha$(H) $C_{29}$ steranes than 5$\alpha$(H),14$\alpha$(H),17$\alpha$(H) $C_{27}$ steranes, while the latter is more enriched in the crude oil from well Wes-2. Similarly, the fraction of the diasteranes is also higher in the condensate. The distribution patterns of terpanes are also significantly different. The Wb-92D condensate has more concentration of Ts than $C_{23}$TT in the *m*/*z* 191 mass chromatogram, with $C_{23}$TT being the highest peak in tricyclic terpane homologues. Compared with gammacerane, the predominance of $C_{30}$ hopane is more obvious. The concentration of $C_{31}$ to $C_{35}$ homohopanes decreases slowly with the increase of the carbon number. In Wes-2 crude oil, $C_{23}$TT is dominant in tricyclic terpane homologues and its concentration is higher than that of Ts. The predominance of $C_{30}$ hopane over gammacerane is smaller than that in condensate. The partial reversal of the homohopanes series occurred with $C_{35}$>$C_{33}$ and $C_{34}$. The ratios or relative concentration parameters of isoprenoids, steranes, and terpanes derived from GC/GC–MS, containing various oil-source correlation information, are listed in Table 3 and analyzed in Section 5.

*4.4. Carbon Isotope.* The shape and trend of the stable carbon isotope type curve can be used to identify the correlation between petroleum and kerogen [96, 97]. The isotopic composition of each fraction will be differentiated during the pyrolysate process of kerogen due to isotopic fractionation, and the carbon isotope will increase with the increasing component polarity and boiling point [98–100]. The carbon isotope sequence of each pyrolysis product approximately shows the following trend [61, 101–104]: saturated hydrocarbon < whole oil < aromatic hydrocarbon < polar hydrocarbon < asphaltene < kerogen.

The $\delta^{13}$C values of the condensates and crude oils are −24.4‰ and−27.1‰, respectively (Table 4). The condensates are isotopically heavier than the crude oils, with a difference of 2.7‰. The $\delta^{13}$C values of EOMs of $J_{1\text{-}2}$ coal-bearing mudstone vary from −26.3‰ to −25.2‰ (average −25.7‰), while that of the $J_2$k-$J_3$o carbonate and gap layer are −27.9‰ to −26.3‰ (average −27.1‰) and −28.2‰ to −26.8‰ (average −27.3‰), respectively. The carbon isotopes of EOMs showed a trend of becoming lighter upward, which also occurred in the kerogens. The $\delta^{13}$C values of $J_{1\text{-}2}$, $J_2$k-$J_3$o, and gap layer kerogen are −25.3‰ to −24.0‰ (average−24.6‰), −27.0‰ to −25.2‰ (average−26.2‰), and −27.4‰ to −26.4‰ (average−26.8‰), respectively. In the source rocks, the $J_{1\text{-}2}$ coal-bearing mudstone shows the typical characteristics of continental organic matter; the carbon isotope of a component in the $J_{1\text{-}2}$ coal-bearing mudstone is isotopically heavier than that of the corresponding component in the gap layer and $J_2$k-$J_3$o carbonate rocks.

## 5. Discussion

*5.1. Thermal Maturity.* The maturity assessment is conducive to unravel the impact of maturity on oil-source correlations. By the quantitative analysis of the diverse molecular biomarkers, the source rocks, condensates, and crude oils of the ADRBB can be distinguished evidently. In this study, two pairs of indicators are selected to assess thermal maturity: $C_{27}$ diasteranes/$C_{27}$ steranes-Ts/Tm [105] and the isomerization index of the $C_{29}$ steranes (Figures 9 and 10). The $C_{27}$ DiaSt/$C_{27}$ St has high sensitivity from early mature to early overmature. The proportion of diasteranes will gradually increase with the increase of maturity [16, 106]. However, it must be pointed out that lithology may affect this parameter [107, 108]. Acidic catalysis is essential in converting sterenes to diasterenes which are the precursors of diasteranes. Therefore, the $C_{27}$ DiaSt/$C_{27}$ St ratio is usually relatively low in carbonate rocks and their generated unmixed petroleum. Bennett and Olsen [109] used $C_{27}$

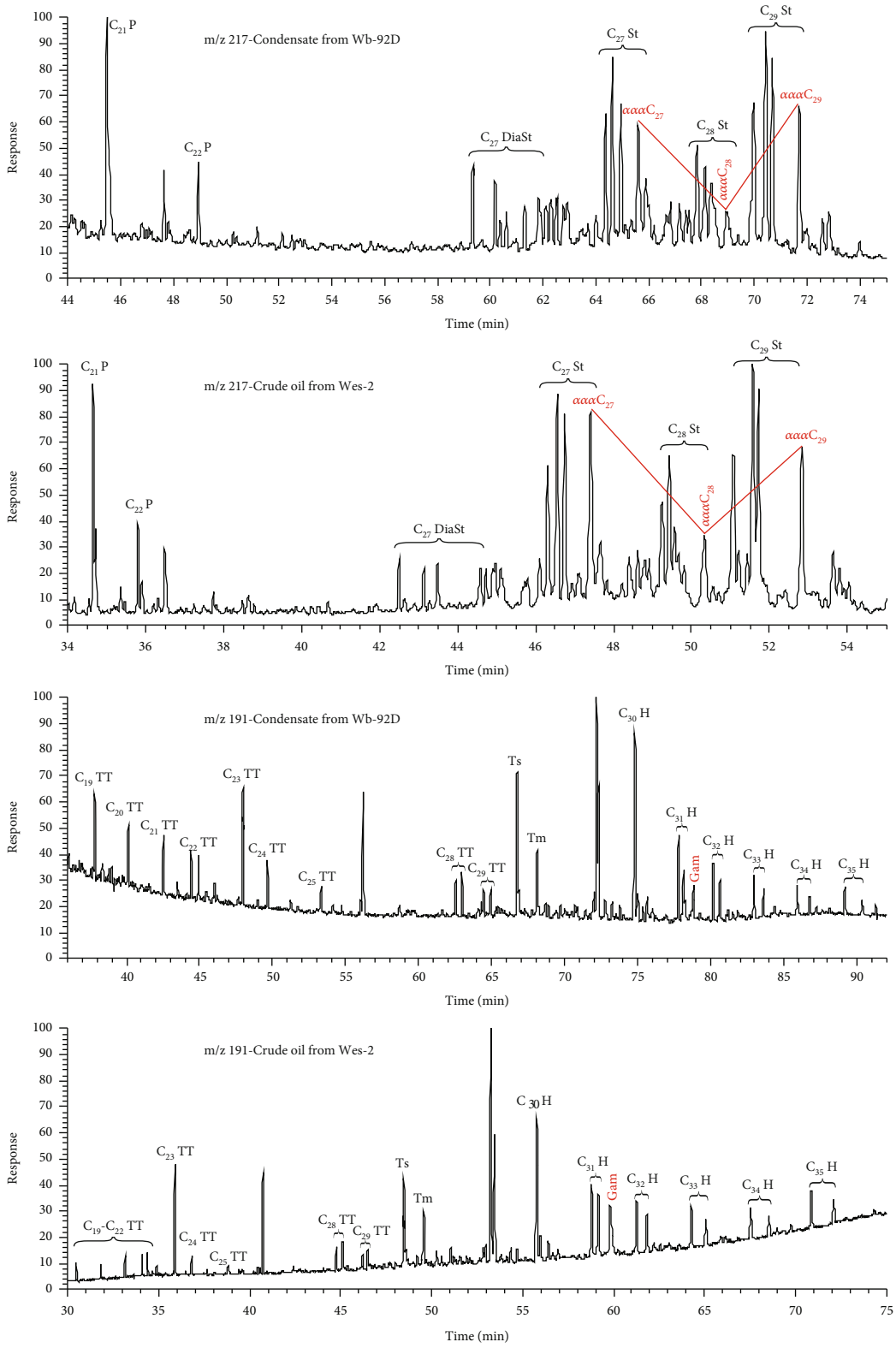


Figure 8: Mass chromatograms of sterane ($m/z = 217$) and terpane ($m/z = 191$) series of saturate fractions for condensates and crude oils. The spectra shown here are for direct comparison purposes. P: pregnane; St: sterane; DiaSt: diasterane; TT: tricyclic terpane; H: hopane; Gam: gammacerane; Ts: 18$\alpha$-trisnorneohopane; Tm: 17$\alpha$-trisnorhopane.

Table 3: Geochemical data of condensates, crude oils, and source rock extracts of the ADRBB.

(a)

| Type & horizon | Well | Depth (m) | Pr/Ph | Pr/n$C_{17}$ | Ph/n$C_{18}$ | $C_{19}$+$C_{20}$TT | $C_{21}$TT | $C_{23}$TT | ETR |
|---|---|---|---|---|---|---|---|---|---|
| Condensate | Wb-92D | 3160 | 1.98 | 0.29 | 0.23 | 45.67 | 23.26 | 31.07 | 0.61 |
| Crude oil | Wes-2 | 3250 | 0.51 | 0.20 | 0.42 | 21.89 | 11.59 | 66.52 | 0.69 |
| EOMs of gap layer | Msa-1 | 3690 | 0.29 | 0.39 | 0.77 | 31.13 | 18.66 | 50.21 | 0.79 |
| | Mc-1 | 3455 | 0.97 | 0.57 | 0.97 | 8.4 | 18.77 | 72.83 | 1.13 |
| | Mc-1 | 3466 | 0.97 | 0.51 | 0.97 | 18.8 | 21.22 | 59.98 | 1.27 |
| | Nye-1 | 3498 | 0.82 | 0.38 | 0.61 | 23.27 | 29.35 | 47.38 | 0.82 |
| | Wb-1 | 3026 | 0.66 | 0.25 | 0.37 | 29.53 | 7.88 | 62.59 | 0.69 |
| | Ejb-1 | 4065 | 0.85 | 0.31 | 0.53 | 20.13 | 22.66 | 57.21 | 1.04 |
| EOMs of $J_2$k-$J_3$o | Msa-1 | 3948 | 0.54 | 0.53 | 0.78 | 24.01 | 34.92 | 41.07 | 0.79 |
| | Sa-2 | 3550 | 0.97 | 1.12 | 0.86 | 18.41 | 37.57 | 44.02 | 1.00 |
| | Sa-2 | 3792 | 0.86 | 0.81 | 0.71 | 22.95 | 42.14 | 34.91 | 0.59 |
| | Mc-1 | 3670 | 0.91 | 1.01 | 0.78 | 35.24 | 24.55 | 40.21 | 0.47 |
| | Soj-1 | 3800 | 0.85 | 0.67 | 0.59 | 34.11 | 38.38 | 27.51 | 0.92 |
| | Soj-1 | 3940 | 1.26 | 0.53 | 0.46 | 30.21 | 34.83 | 34.96 | 0.72 |
| | Nye-1 | 3560 | 1.11 | 0.68 | 0.73 | 28.26 | 34.90 | 36.84 | 0.82 |
| | Nye-1 | 3720 | 0.98 | 0.34 | 0.66 | 29.96 | 32.86 | 37.18 | 0.35 |
| | Wb-1 | 3170 | 0.89 | 0.33 | 0.48 | 32.56 | 35.03 | 32.41 | 0.27 |
| | Wb-16 | 3180 | 0.83 | 1.09 | 0.54 | 16.23 | 29.22 | 54.55 | 1.13 |
| | Ejb-1 | 4320 | 0.90 | 0.57 | 0.59 | 40.88 | 30.50 | 28.62 | 0.69 |
| EOMs of $J_{1\text{-}2}$ | Msa-1 | 3970 | 1.56 | 0.56 | 0.28 | 55.69 | 19.83 | 24.48 | 0.59 |
| | Mc-1 | 3728 | 1.37 | 0.76 | 0.34 | 55.81 | 15.53 | 28.66 | 0.69 |
| | Soj-1 | 4130 | 1.19 | 0.62 | 0.53 | 40.57 | 32.16 | 27.27 | 0.49 |
| | Nye-1 | 3800 | 1.63 | 0.91 | 0.38 | 32.05 | 33.11 | 34.84 | 0.30 |
| | Wb-1 | 3416 | 1.77 | 0.53 | 0.42 | 46.02 | 15.15 | 38.83 | 0.23 |
| | Wb-1 | 3502 | 1.48 | 1.3 | 0.33 | 45.59 | 25.62 | 28.79 | 0.33 |

(b)

| Ts/Tm | $C_{23}$TT/$C_{30}$H | Gam/$C_{30}$H | $St_{27}$ | $St_{28}$ | $St_{29}$ | $C_{27}$DiaSt/$C_{27}$St | $St_{29}$S/(S+R) | $St_{29}\beta\beta/(\beta\beta+\alpha\alpha)$ |
|---|---|---|---|---|---|---|---|---|
| 2.32 | 0.63 | 0.19 | 26.93 | 19.92 | 53.15 | 0.46 | 0.51 | 0.61 |
| 1.13 | 0.31 | 0.34 | 48.29 | 19.13 | 32.58 | 0.19 | 0.45 | 0.47 |
| 1.19 | 0.52 | 0.41 | 53.91 | 18.57 | 27.52 | 0.23 | 0.44 | 0.39 |
| 0.83 | 0.43 | 0.33 | 55.26 | 22.58 | 22.16 | 0.24 | 0.44 | 0.43 |
| 0.75 | 0.44 | 0.38 | 65.16 | 25.32 | 9.52 | 0.31 | 0.41 | 0.39 |
| 0.52 | 0.28 | 0.29 | 61.23 | 13.18 | 25.59 | 0.28 | 0.43 | 0.34 |
| 1.07 | 0.19 | 0.25 | 49.29 | 20.52 | 30.19 | 0.21 | 0.44 | 0.48 |
| 0.87 | 0.32 | 0.28 | 62.95 | 19.56 | 17.49 | 0.22 | 0.45 | 0.36 |
| 1.04 | 0.47 | 0.19 | 35.38 | 28.84 | 35.78 | 0.13 | 0.42 | 0.40 |
| 0.99 | 0.29 | 0.22 | 29.92 | 27.15 | 42.93 | 0.10 | 0.42 | 0.44 |
| 1.13 | 0.38 | 0.13 | 31.52 | 20.21 | 48.27 | 0.06 | 0.46 | 0.38 |
| 1.23 | 0.65 | 0.21 | 42.37 | 22.21 | 35.42 | 0.04 | 0.43 | 0.46 |
| 1.17 | 0.44 | 0.19 | 31.84 | 23.21 | 44.95 | 0.14 | 0.43 | 0.38 |
| 1.26 | 0.41 | 0.22 | 40.36 | 13.12 | 46.52 | 0.15 | 0.45 | 0.39 |
| 0.73 | 0.22 | 0.28 | 44.71 | 25.17 | 30.12 | 0.08 | 0.47 | 0.44 |
| 1.31 | 0.42 | 0.16 | 43.66 | 19.82 | 36.52 | 0.12 | 0.44 | 0.37 |
| 1.42 | 0.17 | 0.15 | 53.08 | 27.13 | 19.79 | 0.07 | 0.45 | 0.45 |

Table 3: Continued.

| Ts/Tm | $C_{23}TT/C_{30}H$ | $Gam/C_{30}H$ | $St_{27}$ | $St_{28}$ | $St_{29}$ | $C_{27}DiaSt/C_{27}St$ | $St_{29}S/(S+R)$ | $St_{29}\beta\beta/(\beta\beta+\alpha\alpha)$ |
|---|---|---|---|---|---|---|---|---|
| 0.95 | 0.58 | 0.14 | 30.20 | 22.52 | 47.28 | 0.14 | 0.45 | 0.37 |
| 1.28 | 0.75 | 0.18 | 29.73 | 18.14 | 52.13 | 0.11 | 0.47 | 0.41 |
| 1.67 | 0.89 | 0.21 | 19.15 | 18.13 | 62.72 | 0.31 | 0.47 | 0.51 |
| 1.82 | 0.85 | 0.15 | 25.11 | 16.12 | 58.77 | 0.33 | 0.49 | 0.50 |
| 1.51 | 0.42 | 0.24 | 37.44 | 12.35 | 50.21 | 0.27 | 0.42 | 0.52 |
| 1.93 | 0.52 | 0.22 | 23.71 | 21.11 | 55.18 | 0.31 | 0.44 | 0.52 |
| 1.74 | 0.72 | 0.19 | 19.61 | 27.11 | 53.28 | 0.32 | 0.48 | 0.49 |
| 1.83 | 0.69 | 0.17 | 15.99 | 22.89 | 61.12 | 0.29 | 0.46 | 0.53 |

Pr: pristine; Ph: phytane; TT: tricyclic terpane; ETR: extended tricyclic terpane ratio; Ts/Tm: 18$\alpha$-trisnorneohopane/17$\alpha$-trisnorhopane; H: hopane; Gam: gammacerane; St: 5$\alpha$(H),14$\alpha$(H),17$\alpha$(H) steranes; DiaSt: diasterane.

Table 4: Isotope data of condensates, crude oils, and source rock extracts of the ADRBB.

| Type & horizon | Well | Depth (m) | EOM/petroleum | Kerogen | *D* value |
|---|---|---|---|---|---|
| Condensate | Wb-92D | 3160 | −24.4 | — | |
| Crude oil | Wes-2 | 3250 | −27.1 | — | |
| Gap layer | Msa-1 | 3690 | −26.8 | −26.4 | 0.4 |
| | Mc-1 | 3455 | −27.3 | −27.0 | 0.3 |
| | Mc-1 | 3466 | −27.6 | −26.8 | 0.8 |
| | Nye-1 | 3498 | −28.2 | −27.4 | 0.8 |
| | Wb-1 | 3026 | −26.9 | −26.6 | 0.3 |
| | Ejb-1 | 4065 | −27.1 | −26.5 | 0.6 |
| $J_2k$-$J_3o$ | Msa-1 | 3948 | −27.7 | −26.9 | 0.8 |
| | Sa-2 | 3550 | −27.9 | −26.5 | 1.4 |
| | Sa-2 | 3792 | −27.6 | −26.7 | 0.9 |
| | Mc-1 | 3670 | −26.9 | −26.1 | 0.8 |
| | Soj-1 | 3800 | −27.0 | −25.2 | 1.8 |
| | Soj-1 | 3940 | −27.3 | −26.4 | 0.9 |
| | Nye-1 | 3560 | −26.3 | −25.6 | 0.7 |
| | Nye-1 | 3720 | −26.5 | −26.0 | 0.5 |
| | Wb-1 | 3170 | −26.6 | −25.9 | 0.7 |
| | Wb-16 | 3180 | −27.1 | −25.8 | 1.3 |
| | Ejb-1 | 4320 | −27.5 | −27.0 | 0.5 |
| $J_{1-2}$ | Msa-1 | 3970 | −25.7 | −24.0 | 1.7 |
| | Mc-1 | 3728 | −26.1 | −25.3 | 0.8 |
| | Soj-1 | 4130 | −25.4 | −24.4 | 1 |
| | Nye-1 | 3800 | −25.2 | −25.0 | 0.2 |
| | Wb-1 | 3416 | −26.3 | −24.8 | 1.5 |
| | Wb-1 | 3502 | −25.5 | −24.2 | 1.3 |

*D* value = $\delta^{13}C$ of kerogen − $\delta^{13}C$ of EOM.

$DiaSt/C_{27}$ St as an indicator of source rock lithology and confirmed this conclusion.

Figure 9 shows that the $C_{27}$ $DiaSt/C_{27}$ St ratio of $J_2k$-$J_3o$ carbonate rocks is the lowest (0.04–0.15) due to lithology (Table 3). The $C_{27}$ $DiaSt/C_{27}$ St ratio of the gap layer and $J_{1-2}$ mudstone positively correlates with Ts/Tm; the deeper the buried depth is, the larger the $C_{27}$ $DiaSt/C_{27}$ St ratios and Ts/Tm ratios are. The $C_{27}$ $DiaSt/C_{27}$ St ratio of the crude oil from well Wes-2 is slightly larger than that of $J_2k$-$J_3o$ carbonate rocks and marginally smaller than that of the gap layer. Simultaneously, its Ts/Tm value is near the median of the two types of rocks, showing a close genetic relationship with the two sets of source rocks. The two ratios of the condensate from Wb-92D are considerably larger than

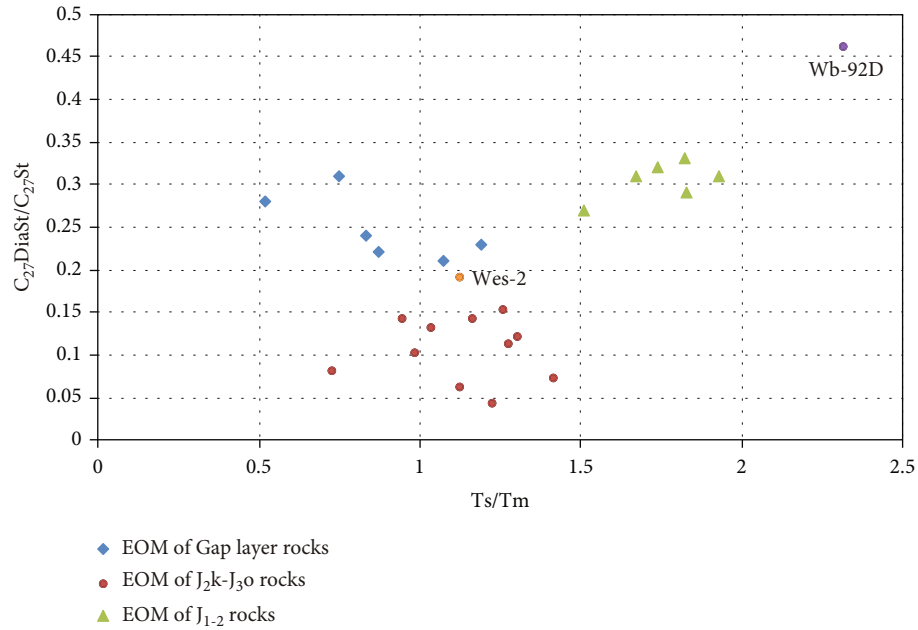


Figure 9: $C_{27}$ DiaSt/$C_{27}$ St versus Ts/Tm for petroleum fluids and source rock EOMs. The $C_{27}$ DiaSt/$C_{27}$ St ratios are calculated from ($C_{27}$ $\beta$, $\alpha$ 20S + 20R diasteranes)/($C_{27}$ $\alpha$, $\beta$, $\beta$ and $\alpha$, $\alpha$, $\alpha$ 20S + 20R steranes). Ts/Tm ratios are calculated from 18$\alpha$-trisnorneohopane over 17$\alpha$-trisnorhopane.

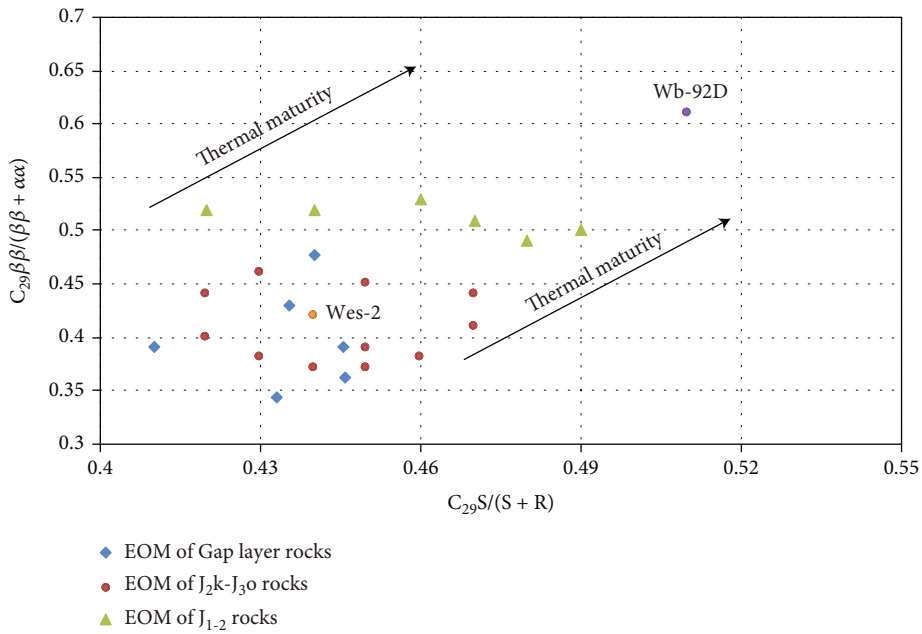


Figure 10: $C_{29}$ $\beta\beta/(\beta\beta+\alpha\alpha)$ versus $C_{29}$ S/(S + R) for petroleum fluids and source rock EOMs. The $C_{29}$ $\beta\beta/(\beta\beta+\alpha\alpha)$ is calculated from ($C_{29}$ $\alpha$, $\beta$, $\beta$ 20S + 20R steranes)/(total $C_{29}$ $\alpha$, $\beta$, $\beta$ 20S + 20R and $C_{29}$ $\alpha$, $\alpha$, $\alpha$ 20S + 20R steranes). The $C_{29}$ S/(S + R) is calculated from ($C_{29}$ $\alpha$, $\alpha$, $\alpha$ 20S steranes)/(total $C_{29}$ $\alpha$, $\alpha$, $\alpha$ 20S + 20R steranes).

those of the source rocks in the ADRBB, showing that it is significantly maturer than the source rocks in the ADRBB. This suggests that the high-maturity condensate from well Wb-92D is not indigenous but migrated products from much deeper levels.

In addition to the $C_{27}$ DiaSt/$C_{27}$ St-Ts/Tm crossplot, the isomerization index of $C_{29}$ steranes can evidently distinguish the source rocks and petroleum [16, 48, 49, 110, 111] (Table 3). The isomerization of $C_{29}$ steranes at the C-14 and C-17 positions makes the $C_{29}$ $\beta\beta/(\beta\beta+\alpha\alpha)$ ratio

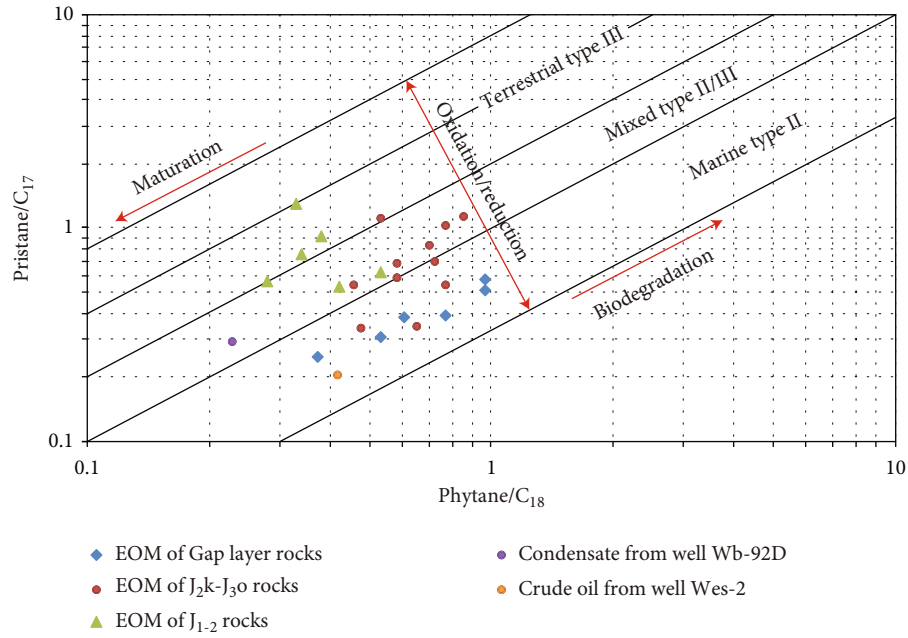


Figure 11: Pristane/nC$_{17}$ versus phytane/nC$_{18}$ for petroleum fluids and source rock EOMs (modified from Shanmugam [112]).

increase from close to 0 to 0.7 with the increasing maturity (the equilibrium value is 0.67–0.71), while the isomerization of C$_{29}$ $\alpha$, $\beta$, $\beta$ steranes at C-20 makes the C$_{29}$ S/(S + R) ratio increase from 0 to about 0.5 with the increasing of maturity (equilibrating at 0.52–0.55) [16]. It can be seen in Figure 10 that the maturity relationship of the three sets of source rocks approximately presents the trend of decreasing upward, which is similar to the trend of Ts/Tm in Figure 9. The J$_2$k-J$_3$o carbonate rocks and the gap layer are mixed together with the crude oil from Wes-2 in the figure, showing a relatively low-maturity state and genetic relationship. However, the C$_{29}$ $\beta\beta/(\beta\beta + \alpha\alpha)$ ratio and the C$_{29}$ S/(S + R) ratio of the condensate from well Wb-92D are significantly higher than those of the source rocks in the ADRBB, indicating that the condensate originates from source rocks with higher maturity.

The result of maturity calculation shows that the condensate from well Wb-92D originated from the source kitchen with higher maturity outside the ADRBB. That is to say, under the premise that the strata are not uplifted and eroded to a large extent and the geothermal gradient is the same, the source kitchen should be the tectonic region in the Amu Darya basin deeper than the ADRBB. According to the existing reports, the source kitchen of the condensates is the Murgab depression. In contrast, the crude oil from well Wes-2 is mainly from the local source rocks of the ADRBB, which is different from the origin of the condensates.

*5.2. Sedimentary Environment and Organic Matter Input.* After the discussion in Section 5.1, it is confirmed that the source rocks in the middle section of the ADRBB are in a low-maturity stage, indicating that the organic matter is relatively close to the original state of sediment. For example, the C$_{29}$ $\beta\beta/(\beta\beta + \alpha\alpha)$ ratio and the C$_{29}$ S/(S + R) ratio of the source rocks have not reached the equilibrium value, which make it possible to identify the sedimentary environment by biomarkers, since the thermal evolution process of organic matter will differentially deplete biomarkers and change the mole percent of components that can indicate the sedimentary environment, leading to the wrong conclusions.

Figure 11 shows a crossplot of ratios of isoprenoids to normal hydrocarbons in Table 3, which validates the sedimentary environment of source rocks and petroleum fluids and determines their maturity [112–114]. The organic matter of J$_{1\text{-}2}$ coal-bearing mudstone is mainly type III kerogen formed by terrestrial organic matter deposition. With the progress of transgression, the seawater continued to be deepening. The J$_2$k-J$_3$o carbonate formed mixed type II/III kerogen from terrestrial and marine organic matter, while the gap layer deposited in the deepest seawater is type II kerogen formed by marine organic matter. According to the analysis in Section 4.2, the two petroleum fluids may be formed by mixed sources. Figure 11 shows that the condensate from well Wb-92D is mostly mixed type II/III, which may come from J$_{1\text{-}2}$ coal-bearing mudstone and J$_2$k-J$_3$o carbonate, and the crude oil from well Wes-2 is primarily marine, which may originate from the gap layer and J$_2$k-J$_3$o carbonate. However, note that the evolution degree of the condensate is separated from the source rocks in the ADRBB, while the evolution degree of the crude oil is well comparable with the samples. This may imply that the condensate migrated from outside the block, and the crude oil is the product of hydrocarbon generation and expulsion of local source rocks.

Although paleosalinity [115] and maturity [116] may have a certain impact on pristane and phytane concentrations, the pristane/phytane (Pr/Ph) ratio is still a helpful parameter to differentiate oxic from anoxic/dysoxic sedimentary environments [16]. It is generally believed that Pr/

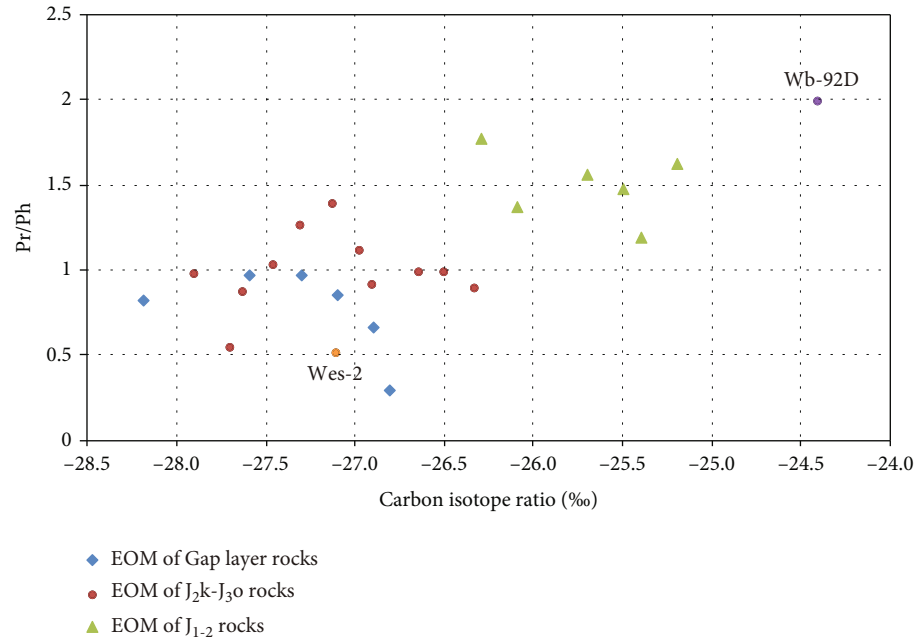


Figure 12: Pr/Ph versus carbon isotope ratio for petroleum fluids and source rock EOMs.

Ph < 1.0 represents the deep and anoxic reducing environment and Pr/Ph > 2.0 indicates the shallow and oxygen-enriched oxidizing environment, while Pr/Ph between 1.0 and 2.0 reflects the transitional weak oxidizing-weak reducing environment. Therefore, Pr/Ph negatively correlates with water depth [16]. Figure 12 shows that the Pr/Ph of $J_{1\text{-}2}$ coal-bearing mudstone is between 1.0 and 2.0, that of $J_2k$-$J_3o$ carbonate is between 0.5 and 1.5, and that of the gap layer is between 0 and 1.0. The water gradually deepens in the evolution process from the sedimentary environment of $J_{1\text{-}2}$ coal-bearing mudstone to the gap layer. The crude oil from well Wes-2 has a relatively low Pr/Ph, which is consistent with the previous understanding that the petroleum fluids with a predominance of even C-numbers have a low Pr/Ph [117], while the condensate from well Wb-92D has a high Pr/Ph, indicating that its parent material is formed in an oxic environment.

The gammacerane index (gammacerane/17$\alpha$,21$\beta$[H]$C_{30}$ hopane) and extended tricyclic terpane ratio (ETR = $[C_{28} + C_{29}]$/Ts) can be used to reflect changes in water salinity/alkalinity through geologic time [54, 118] (Table 3, Figure 13). The gammacerane is believed to be formed by reduction of tetrahymanol originated from bacterivorous ciliates, implying a strong reduction and high-salinity environment [119, 120]. The ETR has been taken to distinguish Jurassic reservoired oil from Triassic as an age-related parameter [121, 122]. ETR is relatively less affected by thermal maturity and biodegradation due to the high thermal stability of $C_{28}$TT, $C_{29}$TT, and Ts to ensure a more accurate interpretation of the parent source. Holba et al. [121] found that the ETR of Triassic oils exceeds 2.0, whereas the Jurassic ETR has lower ratios corresponding to major mass extinction that occurred at the end of the Triassic, which may have altered the principal biological sources of tricyclic terpanes, mostly less than 1.2. Hao et al. [54] observed a relationship between source rocks deposited in deep lake environments and the relative abundance of several terpanes. They pointed out that the high gammacerane index and ETR values are well correlated with source rocks deposited in relatively high salinity zones.

The gammacerane index of the $J_{1\text{-}2}$ coal-bearing mudstone is 0.15–0.24, that of the $J_2k$-$J_3o$ carbonate rocks is 0.19–0.28, and that of the gap layer is 0.25–0.41 (Figure 13). It shows that during the deposition period of the gap layer, the environmental water body of the ADRBB was deep, anoxic, and saline, while the gammacerane index of the $J_{1\text{-}2}$ coal-bearing mudstone and the $J_2k$-$J_3o$ carbonate rocks is relatively low, showing a shallow, oxic, and freshwater body, which is consistent with the conclusions of isoprenoids/normal hydrocarbons in Figure 11 and pristane/phytane in Figure 12. The ETR of the $J_{1\text{-}2}$ coal-bearing mudstone is 0.23–0.69, that of the $J_2k$-$J_3o$ carbonate rocks is 0.27–1.13, and that of the gap layer is 0.69–1.27 (Figure 13). The ETR of all source rocks is less than 1.2, except for one sample of the gap layer. Generally, the ETR of the $J_{1\text{-}2}$ coal-bearing mudstone is the lowest. With the gradual prosperity of organisms after the Triassic mass extinction [123], the ETR of the $J_2k$-$J_3o$ carbonate rocks and gap layer rise again and increase upward. The observed upward increase in the gammacerane index, which is accompanied by an upward increase in ETR and an upward decrease in Pr/Ph ratios, therefore, suggests an evolution of the ADRBB from a shallow-oxic freshwater delta to a deep-anoxic saline marine [2].

Figure 13 shows that the condensate from well Wb-92D has low gammacerane index and medium ETR, which is distributed between the $J_{1\text{-}2}$ coal-bearing mudstone and the $J_2k$-$J_3o$ rocks, indicating that its sedimentary environment is the

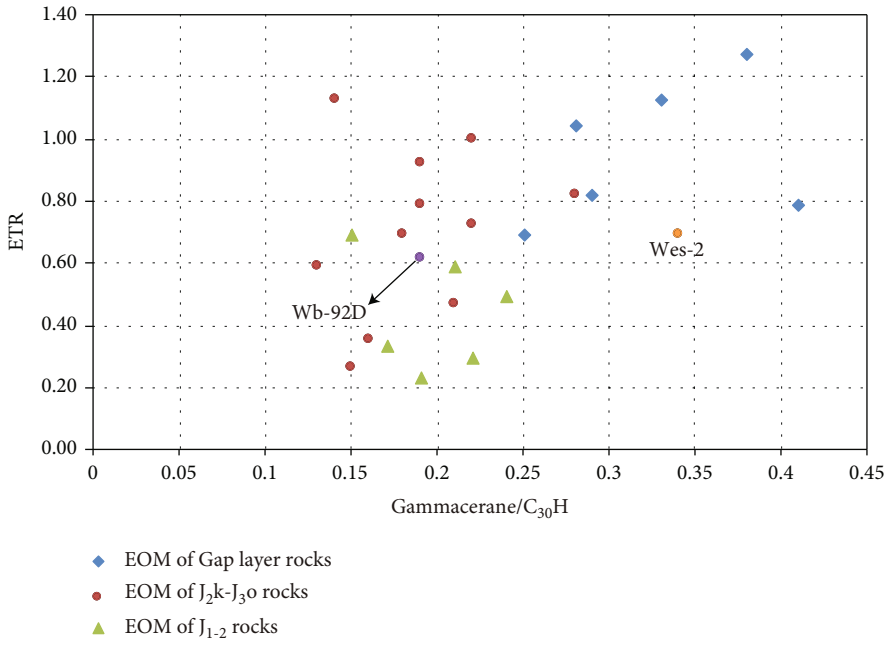


Figure 13: ETR versus gammacerane/$C_{30}$ hopane for petroleum fluids and source rock EOMs.

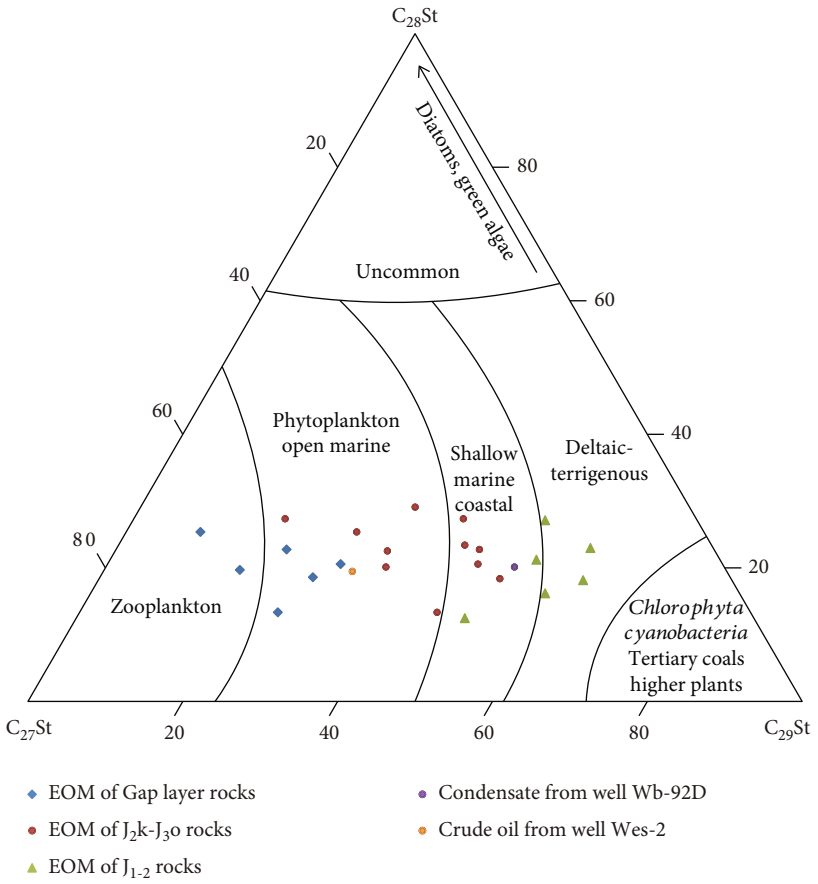


Figure 14: Ternary plot showing the relative proportion of $C_{27}$, $C_{28}$, and $C_{29}$ sterane (St) (5$\alpha$,14$\alpha$,17$\alpha$[H] 20R) (modified from Huang and Meinschein, Liu et al., and Fang et al. [36, 40, 50]).

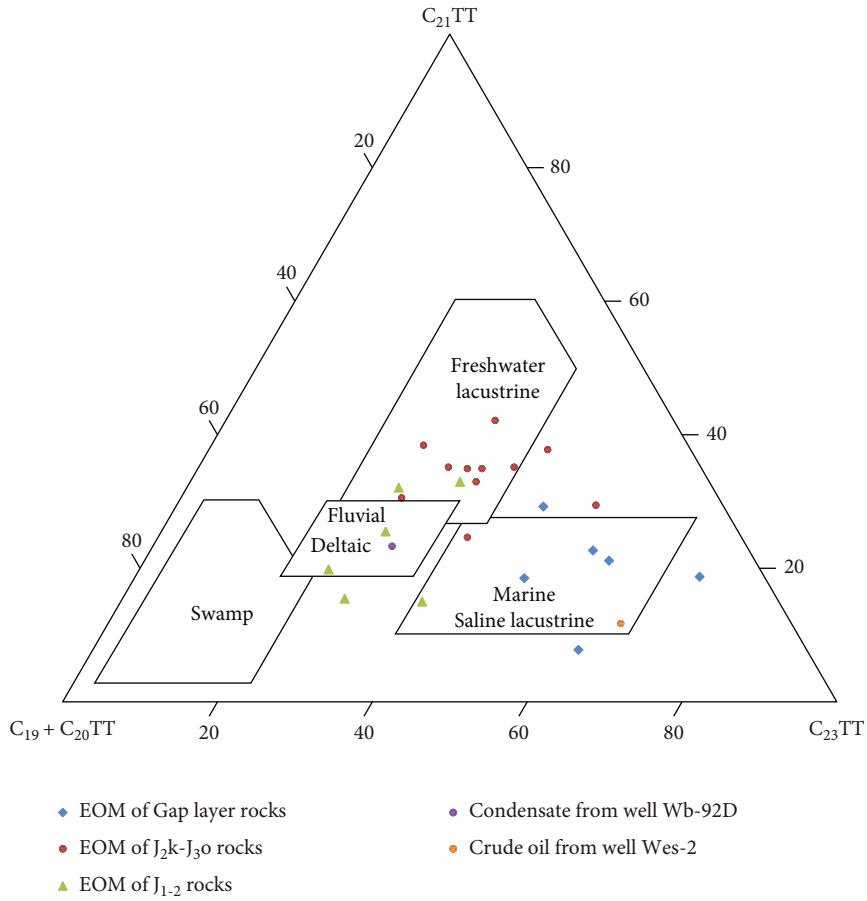


FIGURE 15: Ternary plot showing the relative proportion of $C_{19}$+$C_{20}$, $C_{21}$, and $C_{23}$ tricyclic terpane (TT) (modified from Xiao et al. [45, 46]).

same as these two types of source rocks. The crude oil from well Wes-2 has a gammacerane index as high as that of the gap layer, indicating that the reducing environment plays a controlling role in the formation of the crude oils. The lower ETR value of the crude oils may be caused by mixed source effect.

Steranes originate from sterols in eukaryotes, which occur in algae and higher plants [29, 30]. Either $C_{27}$ steranes or $C_{29}$ steranes usually have the highest relative proportion in the $C_{27}$–$C_{28}$–$C_{29}$ sterane (5$\alpha$,14$\alpha$,17$\alpha$[H] 20R) system due to different sedimentary environments and organic matter input. Generally, $C_{27}$ steranes are derived primarily from marine zooplankton and algae [16, 39, 124] and $C_{29}$ steranes are mainly from terrigenous higher plants, freshwater microalgae, *Chlorophyta*, and *Cyanobacteria* [36–38, 125, 126], whereas $C_{28}$ originates from chlorophyll C-containing phytoplankton, including diatoms, coccolithophores, and dinoflagellates [40, 127, 128]. Furthermore, tricyclic terpanes, which are relatively less affected by maturity and biodegradation, can also be used to identify paleoenvironments. The precursors of tricyclic terpanes are thought to originate mainly from prokaryotic cell membranes [31]. It has also been suggested that the enrichment of tricyclic terpanes is related to the input of marine algae [32–35]. It is generally believed that tricyclic terpanes with low carbon numbers such as $C_{19}$ and $C_{20}$ tricyclic terpanes may come from diterpene precursors, which reflect the input of higher plants which represent terrestrial facies [42, 43]. The sedimentary environment in shallow water may be conducive to the formation and distribution of $C_{19}$ and $C_{20}$ tricyclic terpanes [43]. Typical coal and coal-derived petroleum are rich in $C_{19}$ tricyclic terpanes. The predominance of $C_{23}$ tricyclic terpane concentration is obvious in marine source rocks and oil [44, 129], while the concentration of $C_{21}$ tricyclic terpane is dominant in freshwater lacustrine source rocks and oil [45, 46].

Figures 14 and 15 are ternary plots of the relative proportions of $C_{27}$–$C_{28}$–$C_{29}$ steranes and $C_{19}$+$C_{20}$–$C_{21}$–$C_{23}$ tricyclic terpanes, respectively (Table 3). There is a predominance of $C_{29}$ steranes and $C_{19}$+$C_{20}$ tricyclic terpanes in $J_{1\text{-}2}$ coal-bearing mudstone in respective compound systems ($C_{27}$–$C_{28}$–$C_{29}$ steranes & $C_{19}$+$C_{20}$–$C_{21}$–$C_{23}$ tricyclic terpanes), showing the characteristics of a terrestrial organic matter input. However, the $J_{1\text{-}2}$ coal-bearing mudstone also contains a certain proportion of $C_{27}$ steranes and $C_{23}$ tricyclic terpanes, representing the input of marine organic matter, which is consistent with the sedimentary characteristics of delta in marine-continental transitional facies. On the contrary, the gap layer shows the proportion dominance of $C_{27}$ steranes and $C_{23}$ tricyclic terpanes, indicating that the source of organic matter is mainly marine. The $J_2$k-$J_3$o carbonate rocks are distributed between the $J_{1\text{-}2}$ coal-bearing mudstone and the gap layer, showing that the input of continental organic matter is approximately

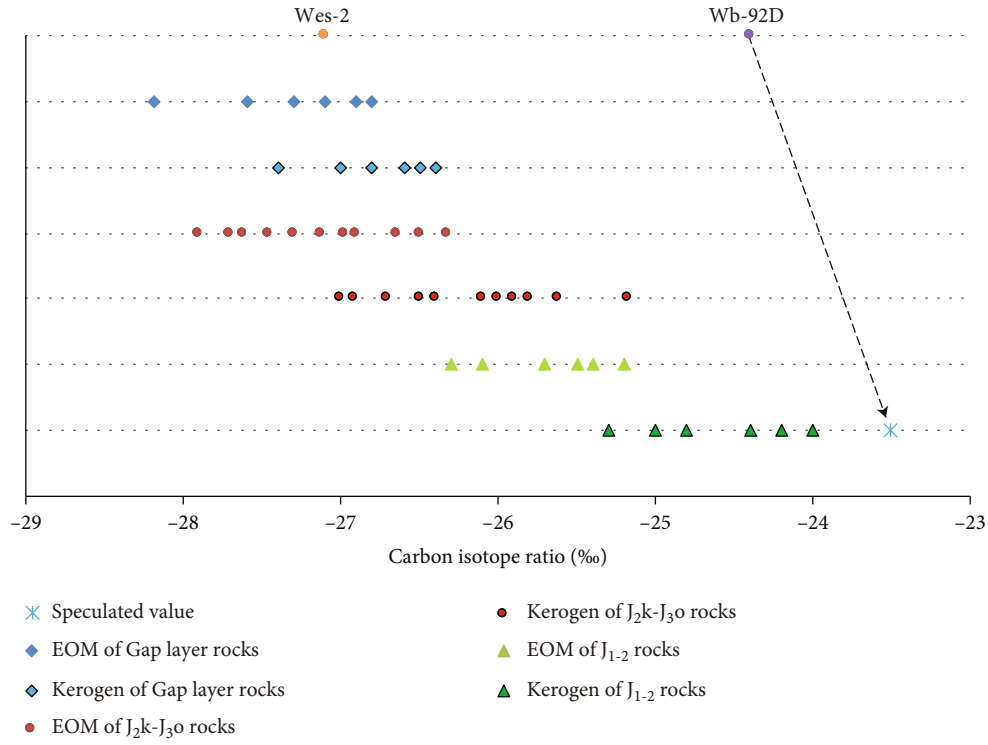


FIGURE 16: Carbon isotopic composition of source rocks and petroleum fluids. The carbon isotopic composition of EOM and petroleum fluids refers to the whole oil.

equal to that of marine organic matter and indicating the process of a continuous deepening of seawater with decreasing continental organic matter input and increasing marine organic matter input from the deposition period of $J_{1\text{-}2}$ coal-bearing mudstone to the deposition period of the gap layer. The projection point of the condensate from well Wb-92D falls in the deltaic-coastal zone with the $J_{1\text{-}2}$ coal-bearing mudstone and the $J_2k\text{-}J_3o$ carbonate samples, whereas the crude oil from well Wes-2 is located in the zone of open marine with gap layer and $J_2k\text{-}J_3o$ carbonate samples. It shows that the condensates originate mainly from the $J_{1\text{-}2}$ coal-bearing mudstone, whereas the crude oils mainly come from the mudstone of the gap layer. And the $J_2k\text{-}J_3o$ carbonate rocks, which are both source rocks and reservoirs, contribute to the formation of the condensates and the crude oils.

*5.3. Isotopic Correlation.* The EOMs and kerogens are significantly depleted in $\delta^{13}C$ compared to the condensate from well Wb-92D (Table 4, Figure 16). The EOM can be regarded as the hydrocarbon generated but has not been expulsed from the source rocks, which means that there is no genetic relationship between the condensates and the source rocks of the ADRBB. Using the average value (0.87‰) of carbon isotope $D$ values between all EOMs and kerogens, the carbon isotope of the parent kerogen of the condensates is speculated (−24.4‰ + 0.87‰ ≈ −23.5‰), since the condensates are hybrid products of $J_{1\text{-}2}$ coal-bearing mudstone, $J_2k\text{-}J_3o$ carbonate rocks, and gap layers. Although the condensates show the characteristics of a mixed source, the speculated value of parent material can be representative to a certain extent. According to the isotope fractionation theory, kerogen will be increasingly $^{13}C$ enriched with increasing maturity. Based on the speculated carbon isotope, the condensate originated from the source rocks with higher maturity, which conforms to the judgment of thermal maturity.

The crude oil from well Wes-2 is isotopically lighter than the condensate, indicating that they are not from a common origin. The $\delta^{13}C$ value of the crude oil is −27.1‰, which is approximately equivalent to that of the EOMs of the gap layer and the $J_2k\text{-}J_3o$ source rocks and less than that of the kerogen of the gap layer and the $J_2k\text{-}J_3o$ source rocks, indicating that the oil from well Wes-2 is the product of the local gap layer and the $J_2k\text{-}J_3o$ carbonate source rocks.

*5.4. Hydrocarbon Accumulation Model.* To better understand petroleum generation, expulsion, and migration history in the right bank block, the tectonic evolution processes were restored on the basis of the seismic data and profiles (Figures 17 and 18). The restored results were carefully examined in the context of the regional geological setting. The evolution process of strata and traps as geological elements of the petroleum system can be observed intuitively through the tectonic evolution process. The oil-source correlation results in this study illustrate the origin and migration direction of hydrocarbon. That is, the gas condensates from the highly mature source rocks in the Murgab depression in the southeast of the Amu Darya basin experienced long-distance lateral migration and accumulated in the ADRBB. In contrast, the newly discovered crude oils

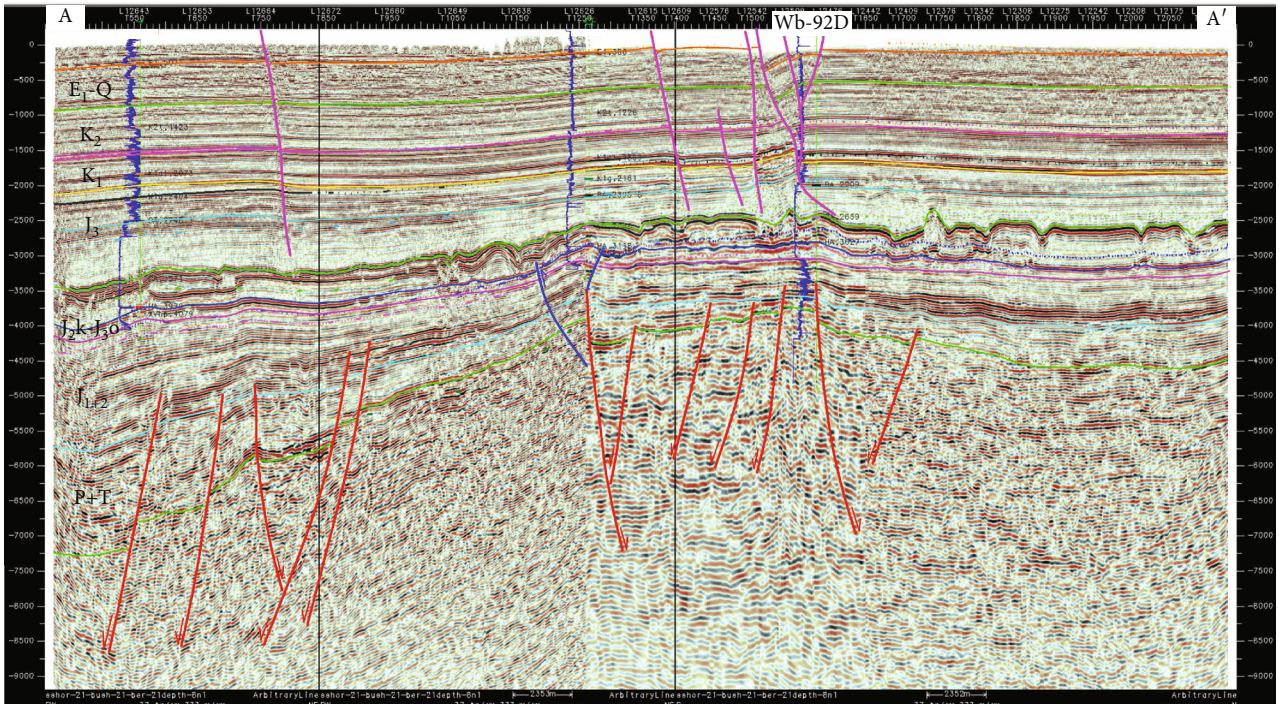


Figure 17: Seismic profile of section A-A′ of the Sandykly uplift in Figure 1.

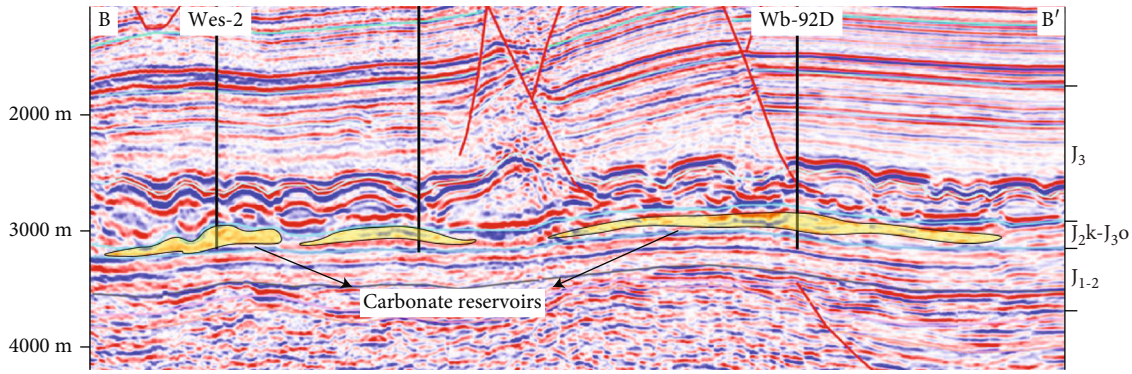


Figure 18: Seismic profile of section B-B′ of the WES gas field in Figure 1.

originate from the local low-maturity source rocks of the ADRBB, which merely experienced short-distance vertical migration and accumulated into $J_2k$-$J_3o$ carbonate reservoirs. Shan et al. [2] identified three hydrocarbon accumulation periods as critical moments of the petroleum system in the middle section of the ADRBB. The accurate hydrocarbon accumulation model can be established by overlaying the migration direction of hydrocarbons originating from various sources on the tectonic evolution profiles at the critical moments of the petroleum system. The hydrocarbon accumulation processes of the WB gas field and WES gas field are summarized as follows:

The carbonate reservoirs and evaporite strata were deposited on the paleo-uplift in the Jurassic Callovian-Oxfordian and Kimmeridgian-Tithonian stages, respectively, and traps that could capture the passing hydrocarbon were formed at the WB gas field and WES gas field [66, 80].

At the end of the early Cretaceous, the hydrocarbon generated in the deeply buried Murgab depression in the southeast of the Amu Darya basin migrated to the Sandykly uplift on the ADRBB along the unconformity between the Jurassic strata and the basement and the fault running through the basement [1]. Then, the of WB gas field traps captured the hydrocarbon from outside the block to form the first-generation oil and gas reservoir (Figure 19(a)). However, due to the lack of basement faults in the WES gas field, there is no effective migration path between the hydrocarbon migrating from the Murgab depression and the reservoir, making it difficult for the traps of the WES gas field to capture the hydrocarbon to form a reservoir. That is, under the background that hydrocarbon from the Murgab depression was massively charging the middle reservoirs on the ADRBB, the reservoir of the WES gas field remained in the state of "empty trap."

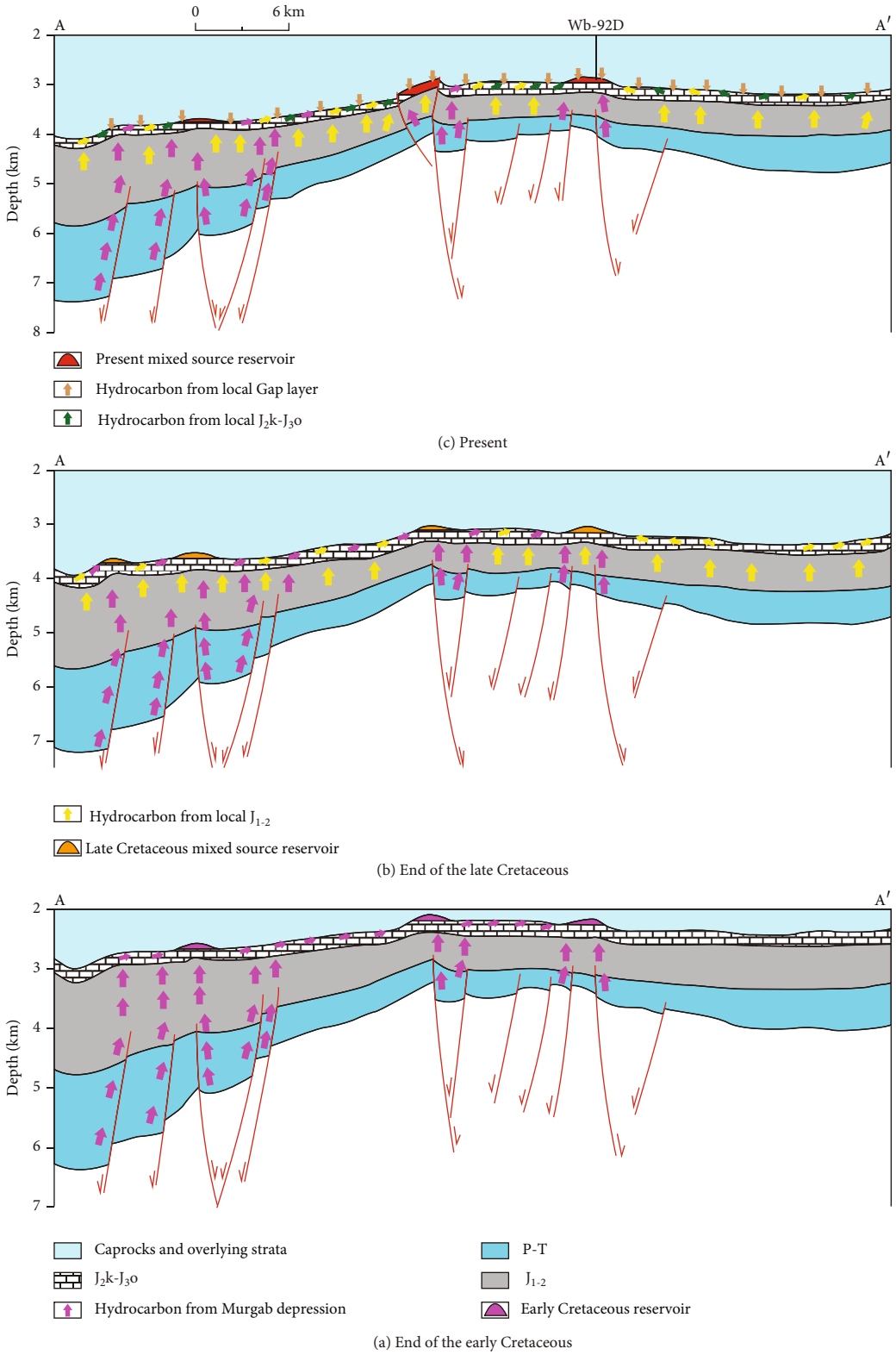


Figure 19: Tectonic evolution and reservoir formation profile of the WB gas field.

At the end of the late Cretaceous, the $J_{1\text{-}2}$ coal-bearing source rocks in the Murgab depression entered the condensate window and generated and expelled a large amount of condensate gas which originated from thermal-cracking oil and kerogen [1]. The condensate gas continued to charge the WB gas field. Meanwhile, the $J_{1\text{-}2}$ coal-bearing mudstone of the ADRBB reached the mature state and entered the oil window. The generated hydrocarbon began to migrate upward into the carbonate reservoirs driven by buoyancy. In the WB gas field, the hydrocarbon generated locally

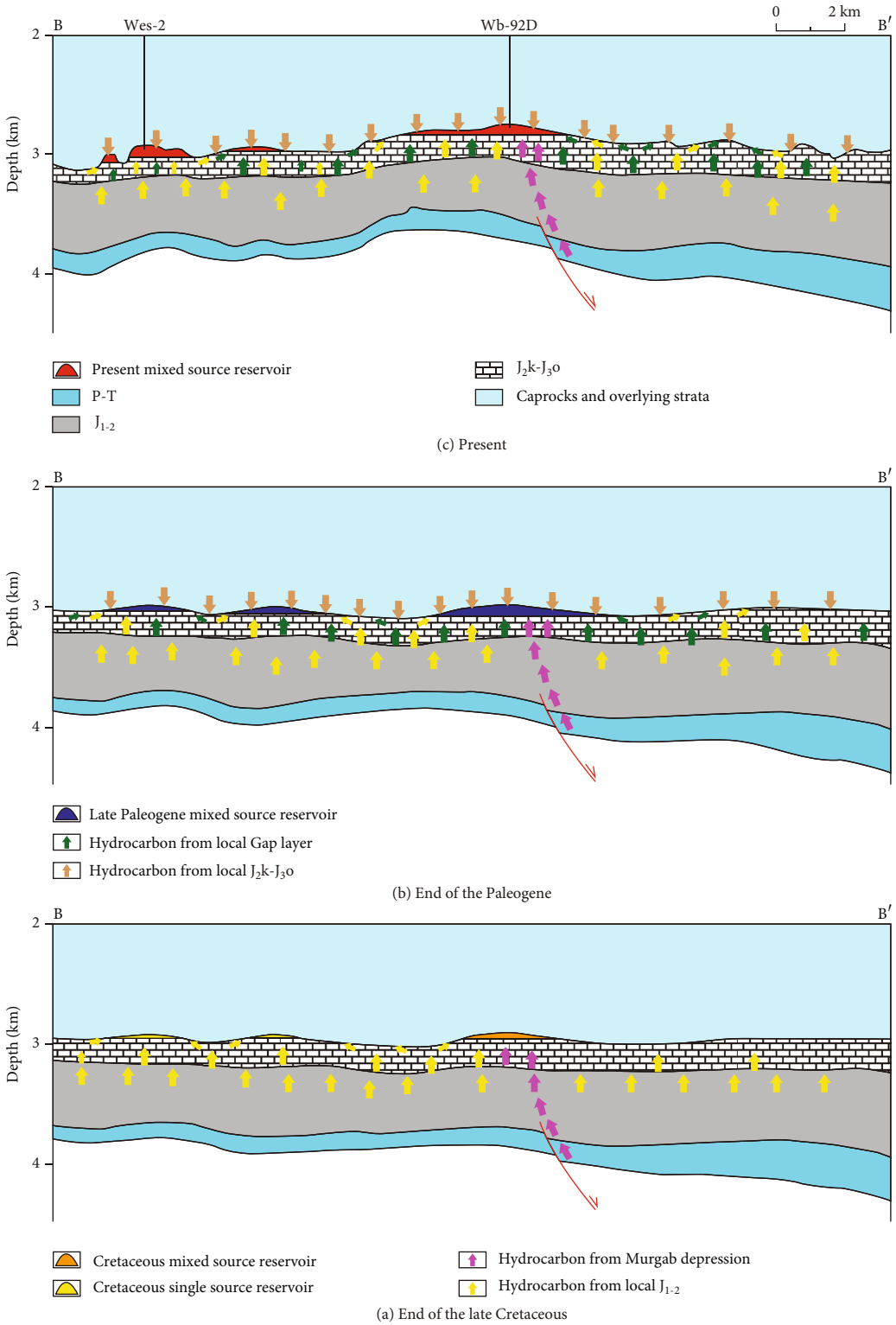


Figure 20: Tectonic evolution and reservoir formation profile of the WES gas field.

charged the reservoir together with the condensate gas migrating from the Murgab depression to form the second-generation oil and gas reservoir (Figure 19(b)). In the WES gas field, the trap prevented the upward migration of the hydrocarbon from $J_{1\text{-}2}$ coal-bearing mudstone of the ADRBB and enriched hydrocarbon in situ (Figure 20(a)).

At the end of the Paleogene, the Callovian-Oxfordian carbonate strata and gap layer mudstone of the ADRBB entered the oil window and began hydrocarbon generation. The carbonates were both source rocks and reservoirs whose hydrocarbon production only needed to migrate to the high point of traps along the structural ridge in the carbonate strata to

accumulate. The gap layer mudstone was covered by thick and dense evaporite rock series, which blocked the upward migration of the hydrocarbon generated by the gap layer. Driven by the internal pressure, the hydrocarbon was expelled into the lower carbonate rocks. The hydrocarbon generated by the carbonate rocks and gap layer was mixed with the oil and gas that have accumulated into reservoirs, forming the third-generation oil and gas reservoir (Figure 20(b)).

In the Neogene Period, the ADRBB experienced Himalayan orogeny [65], which changed and adjusted the carbonate traps, some were destroyed by faulting, and some were strengthened by the increase in closure height. It can be seen from the profiles that the Himalayan orogeny resulted in the formation of fault blocks in the south of the WB gas field (Figure 19(c)). And the WB gas field and the WES gas field were subjected to tectonic compression of orogeny, which enhanced the amplitude of the anticline and increased the volume of traps to accommodate more oil and gas (Figure 20(c)).

After the Himalayan orogeny, the ADRBB has not experienced large tectonic movement so that the hydrocarbon reservoirs can be well preserved up to now (Figures 19(c) and 20(c)). In the traps with developed basement faults, such as the WB gas field, the geochemical indices show the characteristics of high maturity, indicating that the oil and gas generated in the Murgab depression were the main sources to continuously charge the traps, while the oil and gas generated by the source rocks in the local depression of the ADRBB were the secondary. In the traps with undeveloped basement faults, such as the WES gas field, the traps mainly captured the oil and gas generated by the local depression of the ADRBB.

## 6. Conclusions

The comprehensive geochemical index comparison provides insight into the sedimentary environment, organic matter input, and thermal maturity of the ADRBB source rocks and petroleum. It is considered that the source of the condensate from well Wb-92D is mainly $J_{1\text{-}2}$ coal-bearing mudstone, supplemented by $J_2k$-$J_3o$ carbonate rocks. However, the maturity of the condensate is significantly higher than that of the local source rocks, indicating that the condensate should originate from the Murgab depression and accumulated in the ADRBB. The recently discovered crude oil from well Wes-2 mainly comes from the gap layer mudstone, followed by the $J_2k$-$J_3o$ carbonate rocks, and its maturity and carbon isotope are comparable with the local source rocks. The WES hydrocarbon reservoir is typically formed by the local source rocks.

According to the shape and the formation process of the current hydrocarbon reservoirs in the middle section of the ADRBB, the crude oils which are the same as those of well Wes-2 may be accumulated in the traps with undeveloped basement faults. The traps with developed basement faults are charged with condensates and natural gas from Murgab depression. Due to the difference in density, the crude oils generated from local source rocks cannot displace the condensates and natural gas in these traps. For the traps with undeveloped basement faults, the oil and gas from the Murgab depression cannot be charged due to the lack of an effective migration channel. So, the crude oils originating from local source rocks can accumulate in these "empty traps" driven by buoyancy and capillary force. Exploring the high structural position of carbonate reservoirs without basement faults, which are located at the transition position between depression and uplift, the explorers may find the new commercial crude oil reservoirs.

## Data Availability

The organic geochemical data used to support the findings of this study are included within the article.

## Conflicts of Interest

The authors declare that they have no conflicts of interest.

## Authors' Contributions

Yunpeng Shan analyzed the geochemical data and wrote the paper; Hui Chai pointed out the demand for geochemical analysis and obtained the permission of Turkmenistan to publish this article; Hongjun Wang provided the samples and designed the study; Liangjie Zhang and Penghui Su polished the English language; Xiangwen Kong drew the figures; Zhenhua Bai searched the literatures; Muwei Cheng and Hongwei Zhang organized the article format.

## Acknowledgments

This study was supported by the National Major Science and Technology Projects of China (Grant no. 2016ZX05029005) and the Technology Research Projects of CNPC (Grant no. 2021DJ33). We thank CNPC (Turkmenistan) Amu Darya gas company for kindly providing samples in this study.

## References

[1] G. F. Ulmishek*Petroleum geology and resources of the Amu-Darya Basin, Turkmenistan, Uzbekistan, Afghanistan, and Iran*2201U.S. Geological Survey Bulletin, 2004.

[2] Y. P. Shan, H. J. Wang, L. J. Zhang, P. H. Su, M. W. Cheng, and Z. H. Bai, "Study on hydrocarbon accumulation periods based on fluid inclusions and diagenetic sequence of the subsalt carbonate reservoirs in the Amu Darya Right Bank Block," *Geofluids*, vol. 2022, Article ID 2412615, 19 pages, 2022.

[3] B. X. Lu, R. C. Zheng, S. C. Chen, F. B. Xu, Q. B. Wen, and H. G. Wen, "Characteristics of carbonate reservoir in Oxfordian of Odjarly Gasfield, Amu Darya Basin," *Journal of Guilin University of Technology*, vol. 31, pp. 505–510, 2011, (in Chinese with English abstract).

[4] W. L. Xu, R. C. Zheng, H. Y. Fei et al., "Characteristics and timing of fractures in the Callovian-0xfordian boundary of the right bank of the Amu Darya River, Turkmenistan," *Natural Gas Industry*, vol. 32, pp. 33–38, 2012, (in Chinese with English abstract).

[5] M. L. Nie, L. Wu, S. B. Xu, and B. Liu, "Genetic mechanism and exploration significance of tectonic action in the

Bieshikent Depression and its adjacent area in the Amu-Darya Basin," *Natural Gas Industry*, vol. 33, pp. 45–50, 2013, (in Chinese with English abstract).

[6] M. L. Nie, S. B. Xu, L. Wu, J. Y. He, H. H. Ming, and R. Zhang, "Features of gas reservoirs in subsalt faulted reef complex in the right bank of the Amu Darya River, Turkmenistan, and their significance in exploration: a case study of the BP gas reservoir," *Natural Gas Industry*, vol. 35, pp. 24–29, 2015, (in Chinese with English abstract).

[7] R. C. Zheng, Y. Li, L. Wu, X. Z. Wu, F. J. Li, and G. Niu, "Geochemical characteristics of Callovian-Oxfordian carbonates in Samandepe gas field, Amu Darya Basin, Turkmenistan," *Petroleum Science*, vol. 8, no. 4, pp. 371–381, 2011.

[8] R. C. Zheng, Y. H. Pan, C. Zhao, L. Wu, and R. Yang, "Carbon and oxygen isotope stratigraphy of the Oxfordian carbonate rocks in Amu Darya basin," *Journal of Earth Science*, vol. 24, no. 1, pp. 42–56, 2013.

[9] Q. Wang, X. Z. Wang, J. L. Xu, B. Liu, and Q. Zhang, "Carbon and oxygen isotope stratigraphy research in Chashgui area," *Journal of Southwest Petroleum University (Science & Technology Edition)*, vol. 36, pp. 27–34, 2014, (in Chinese with English abstract).

[10] J. D. Brooks, K. Gould, and J. W. Smith, "Isoprenoid hydrocarbons in coal and petroleum," *Nature*, vol. 222, no. 5190, pp. 257–259, 1969.

[11] G. R. S. Júnior, A. L. S. Santos, S. G. Lima et al., "Evidence for euphotic zone anoxia during the deposition of Aptian source rocks based on aryl isoprenoids in petroleum, Sergipe-Alagoas Basin, northeastern Brazil," *Organic Geochemistry*, vol. 63, pp. 94–104, 2013.

[12] V. C. M. Góes, A. B. Costa, C. L. N. Andrade et al., "Hydrocarbon source potential and paleodepositional environment of the (Devonian) Barreirinha formation on the south edge of the Amazonas basin border, Brazil," *Journal of South American Earth Sciences*, vol. 115, article 103722, 2022.

[13] M. Mei, K. K. Bissada, T. B. Malloy, L. M. Darnell, and Z. F. Liu, "Origin of condensates and natural gases in the Almond Formation reservoirs in southwestern Wyoming, USA," *Organic Geochemistry*, vol. 124, pp. 164–179, 2018.

[14] L. D. C. González, J. G. M. Filho, and M. Mastalerz, "Depositional environment and maturity of Devonian Pimenteira Formation in the Sao Luis Basin, Brazil," *International Journal of Coal Geology*, vol. 221, article 103429, 2020.

[15] J. G. Lu, J. B. Liao, X. J. Liu et al., "Geochemistry of different source rocks and oil-source correlation of lacustrine sedimentary successions: a case study of the Triassic Yanchang formation in the Dingbian-Wuqi area, Ordos Basin, northern China," *Journal of Asian Earth Sciences*, vol. 232, article 105216, 2022.

[16] K. E. PetersC. C. Walters, andJ. M. Moldowan*The Biomarker Guide: Biomarkers and Isotopes in the Environment and Human History*2, Cambridge University Press, New York, 2005.

[17] R. C. Clark and M. Blumer, "Distribution of *n*-paraffins in marine organisms and sediment1," *Limnology & Oceanography*, vol. 12, no. 1, pp. 79–87, 1967.

[18] G. L. Wang, Y. C. Xue, D. W. Wang, S. B. Shi, K. Grice, and P. F. Greenwood, "Biodegradation and water washing within a series of petroleum reservoirs of the Panyu oil field," *Organic Geochemistry*, vol. 96, pp. 65–76, 2016.

[19] Z. Chai, Z. H. Chen, H. Liu et al., "Light hydrocarbons and diamondoids of light oils in deep reservoirs of Shuntuoguole Low Uplift, Tarim Basin: implication for the evaluation on thermal maturity, secondary alteration and source characteristics," *Marine and Petroleum Geology*, vol. 117, article 104388, 2020.

[20] V. Aghadadashi, A. Mehdinia, and S. Molaei, "Normal alkanes in sediments from the Persian Gulf: spatial pattern and implications for autochthonous, allochthonous, and petroleum-originated contaminants," *Environmental Monitoring and Assessment*, vol. 193, no. 6, p. 364, 2021.

[21] F. Froidl, R. Littke, A. Baniasad et al., "Peculiar Berriasian "Wealden" Shales of northwest Germany: organic facies, depositional environment, thermal maturity and kinetics of petroleum generation," *Marine and Petroleum Geology*, vol. 124, article 104819, 2021.

[22] M. Luemba, Z. H. Chen, and J. Ntibahanana, "Molecular markers of Neoproterozoic-Lower Paleozoic petroleum systems and their geological significance: a case study of the cratonic basins in western China," *Journal of Petroleum Science and Engineering*, vol. 204, article 108707, 2021.

[23] M. A. Gough, M. M. Rhead, and S. J. Rowland, "Biodegradation studies of unresolved complex mixtures of hydrocarbons: model UCM hydrocarbons and the aliphatic UCM," *Organic Geochemistry*, vol. 18, no. 1, pp. 17–22, 1992.

[24] C. F. Cai, C. M. Zhang, L. L. Cai et al., "Origins of Palaeozoic oils in the Tarim Basin: evidence from sulfur isotopes and biomarkers," *Chemical Geology*, vol. 268, no. 3-4, pp. 197–210, 2009.

[25] T. C. Tran, G. A. Logan, E. Grosjean, D. Rtan, and P. J. Marriott, "Use of comprehensive two-dimensional gas chromatography/time-of-flight mass spectrometry for the characterization of biodegradation and unresolved complex mixtures in petroleum," *Geochimica et Cosmochimica Acta*, vol. 74, no. 22, pp. 6468–6484, 2010.

[26] S. Z. Hu, S. F. Li, J. H. Wang, and J. Gao, "Origin of unresolved complex mixtures (UCMs) in biodegraded oils: insights from artificial biodegradation experiments," *Fuel*, vol. 231, pp. 53–60, 2018.

[27] M. Zhang, C. L. Liu, J. X. Tian et al., "Geochemical characteristics of crude oil and oil-source correlation in the western Qaidam Basin, China," *Journal of Natural Gas Geoscience*, vol. 5, no. 4, pp. 227–238, 2020.

[28] K. F. M. Thompson, "Hybrid gas condensates and the evolution of their volatile light hydrocarbons," *Organic Geochemistry*, vol. 93, pp. 32–50, 2016.

[29] W. K. Seifert and J. M. Moldowan, "Use of biological markers in petroleum exploration," in *Biological Markers in the Sedimentary Record*, R. B. Johns, Ed., pp. 261–290, Elsevier, Amsterdam, 1986.

[30] L. Schwark and P. Empt, "Sterane biomarkers as indicators of palaeozoic algal evolution and extinction events," *Palaeogeography Palaeoclimatology Palaeoecology*, vol. 240, no. 1-2, pp. 225–236, 2006.

[31] G. Ourisson, P. Albrecht, and M. Rohmer, "Predictive microbial biochemistry – from molecular fossils to procaryotic membranes," *Trends in Biochemical Sciences*, vol. 7, no. 7, pp. 236–239, 1982.

[32] F. R. A. Neto, A. Restle, J. Connan, P. Albrecht, and G. Ourisson, "Novel tricyclic terpanes ($C_{19}$, $C_{20}$) in sediments and petroleums," *Tetrahedron Letters*, vol. 23, no. 19, pp. 2027–2030, 1982.

[33] B. R. T. Simoneit, R. N. Leif, F. R. A. Neto, D. A. Azevedo, A. C. Pinto, and P. Albrecht, "On the presence of tricyclic terpane hydrocarbons in permian tasmanite algae," *Naturwissenschaften*, vol. 77, no. 8, pp. 380–383, 1990.

[34] B. R. T. Simoneit, M. Schoell, R. F. Dias, and F. R. A. Neto, "Unusual carbon isotope compositions of biomarker hydrocarbons in a Permian tasmanite," *Geochimica et Cosmochimica Acta*, vol. 57, no. 17, pp. 4205–4211, 1993.

[35] S. M. B. D. Grande, F. R. A. Neto, and M. R. Mello, "Extended tricyclic terpanes in sediments and petroleums," *Organic Geochemistry*, vol. 20, no. 7, pp. 1039–1047, 1993.

[36] W. Y. Huang and W. G. Meinschein, "Sterols as ecological indicators," *Geochimica et Cosmochimica Acta*, vol. 43, no. 5, pp. 739–745, 1979.

[37] J. K. Volkman, "A review of sterol markers for marine and terrigenous organic matter," *Organic Geochemistry*, vol. 9, no. 2, pp. 83–99, 1986.

[38] M. Farhaduzzaman, W. H. Abdullah, and M. A. Islam, "Depositional environment and hydrocarbon source potential of the Permian Gondwana coals from the Barapukuria Basin, Northwest Bangladesh," *International Journal of Coal Geology*, vol. 90-91, pp. 162–179, 2012.

[39] Y. D. Zhang, A. J. Jiang, Y. G. Sun, L. J. Xie, and P. X. Chai, "Stable carbon isotope compositions of isoprenoid chromans in Cenozoic saline lacustrine source rocks from the Western Qaidam Basin, NW China: source implications," *Chinese Science Bulletin*, vol. 57, no. 9, pp. 1013–1023, 2012.

[40] B. Liu, A. Bechtel, R. F. Sachsenhofer, D. Gross, R. Gratzer, and X. Chen, "Depositional environment of oil shale within the second member of Permian Lucaogou Formation in the Santanghu Basin, Northwest China," *International Journal of Coal Geology*, vol. 175, pp. 10–25, 2017.

[41] M. W. Alkhafaji, J. Connan, M. H. Engel, and S. W. Al-Jubouri, "Origin, biodegradation, and water washing of bitumen from the Mishraq Sulfur Mine, northern Iraq," *Marine and Petroleum Geology*, vol. 124, article 104786, 2021.

[42] C. M. Ekweozor and O. P. Strausz, "Tricyclic terpanes in the Athabasca oil sands: their geochemistry," in *Advances in Organic Geochemistry*, M. Bjorøy, P. Albrecht, C. Cornford, K. Groot, G. Eglinton, E. Galimov, D. Leythaeuser, R. Pelet, J. Rullkötter, and G. Speers, Eds., pp. 746–766, John Wiley & Sons, Chichester, 1983.

[43] J. E. Zumberge, "Prediction of source rock characteristics based on terpane biomarkers in crude oils: a multivariate statistical approach," *Geochimica et Cosmochimica Acta*, vol. 51, no. 6, pp. 1625–1637, 1987.

[44] S. Z. Tao, C. Y. Wang, J. G. Du, L. Liu, and Z. Chen, "Geochemical application of tricyclic and tetracyclic terpanes biomarkers in crude oils of NW China," *Marine and Petroleum Geology*, vol. 67, pp. 460–467, 2015.

[45] H. Xiao, M. J. Li, W. Q. Wang et al., "Identification, distribution and geochemical significance of four rearranged hopane series in crude oil," *Organic Geochemistry*, vol. 138, article 103929, 2019.

[46] H. Xiao, M. J. Li, Z. Yang, and Z. L. Zhu, "Distribution patterns and geochemical implications of C19-C23 tricyclic terpanes in source rocks and crude oils occuring in various depositional environments," *Acta Geochimica*, vol. 48, pp. 161–170, 2019, (in Chinese with English abstract).

[47] A. Z. Rabbani, J. Sadouni, and M. Asemani, "Chemometric investigation of oil families and geochemical characterization of crude oils in the Northern Dezful Embayment Zone, SW Iran," *Journal of Petroleum Science and Engineering*, vol. 214, article 110496, 2022.

[48] H. Justwan, B. Dahl, and G. H. Isaksen, "Geochemical characterisation and genetic origin of oils and condensates in the South Viking Graben, Norway," *Marine and Petroleum Geology*, vol. 23, no. 2, pp. 213–239, 2006.

[49] S. Y. Yang, H. M. Schulz, N. H. Schovsbo, and J. A. Bojesen-Koefoed, "Oil-source-rock correlation of the Lower Paleozoic petroleum system in the Baltic Basin (northern Europe)," *American Association of Petroleum Geologists Bulletin*, vol. 101, no. 12, pp. 1971–1993, 2017.

[50] R. H. Fang, R. Littke, L. Zieger, A. Baniasad, M. J. Li, and J. Schwarzbauer, "Changes of composition and content of tricyclic terpane, hopane, sterane, and aromatic biomarkers throughout the oil window: a detailed study on maturity parameters of Lower Toarcian Posidonia Shale of the Hils Syncline, NW Germany," *Organic Geochemistry*, vol. 138, article 103928, 2019.

[51] E. A. Mehmandosti, M. Amirhoseyni, S. A. Moallemi, and A. Habibi, "Geochemical investigation of the Cretaceous crude oil reservoirs and source rock samples in one of the Abadan Plain Oilfields, SW Iran," *Acta Geologica Sinica*, vol. 96, no. 2, pp. 546–558, 2022.

[52] J. M. Bravo, M. Perzl, T. Härtner, E. L. Kannenberg, and M. Rohmer, "Novel methylated triterpenoids of the gammacerane series from the nitrogen-fixing bacterium *Bradyrhizobium japonicum* USDA 110," *European Journal of Biochemistry*, vol. 268, no. 5, pp. 1323–1331, 2001.

[53] J. S. Sinninghe Damsté and J. W. De Leeuw, "Comments on "biomarkers or not biomarkers. A new hypothesis for the origin of pristane involving derivation from methyltrimethyltridecylchromans (MTTCs) formed during diagenesis from chlorophyll and alkylphenols" from M. Li, S. R. Larter, P. Taylor, D. M. Jones, B. Bowler and M. Bjorøy," *Organic Geochemistry*, vol. 23, no. 11-12, pp. 1085–1087, 1995.

[54] F. Hao, X. H. Zhou, Y. M. Zhu, and Y. Y. Yang, "Lacustrine source rock deposition in response to co-evolution of environments and organisms controlled by tectonic subsidence and climate, Bohai Bay Basin, China," *Organic Geochemistry*, vol. 42, no. 4, pp. 323–339, 2011.

[55] A. Bechtel, J. Jia, S. A. I. Strobl et al., "Palaeoenvironmental conditions during deposition of the Upper Cretaceous oil shale sequences in the Songliao Basin (NE China): implications from geochemical analysis," *Organic Geochemistry*, vol. 46, pp. 76–95, 2012.

[56] S. Tulipani, K. Grice, P. F. Greenwood et al., "Molecular proxies as indicators of freshwater incursion-driven salinity stratification," *Chemical Geology*, vol. 409, pp. 61–68, 2015.

[57] X. J. Ding, C. H. Gao, M. Zha, H. Chen, and Y. Su, "Depositional environment and factors controlling $\beta$-carotane accumulation: a case study from the Jimsar Sag, Junggar Basin, northwestern China," *Palaeogeography, Palaeoclimatology, Palaeoecology*, vol. 485, pp. 833–842, 2017.

[58] Z. Sofer, "Stable carbon isotope compositions of crude oils: application to source depositional environments and petroleum alteration," *American Association of Petroleum Geologists Bulletin*, vol. 68, pp. 31–49, 1984.

[59] C. F. Cai, C. M. Zhang, R. H. Worden et al., "Application of sulfur and carbon isotopes to oil-source rock correlation: a case study from the Tazhong area, Tarim Basin, China," *Organic Geochemistry*, vol. 83-84, pp. 140–152, 2015.

[60] A. I. Holman and K. Grice, "$\delta^{13}$C of aromatic compounds in sediments, oils and atmospheric emissions: a review," *Organic Geochemistry*, vol. 123, pp. 27–37, 2018.

[61] Q. S. Sun, F. Xiao, X. Y. Gao et al., "A new discovery of Mesoproterozoic erathem oil, and oil-source correlation in the Niuyingzi area of western Liaoning Province, NE China," *Marine and Petroleum Geology*, vol. 110, pp. 606–620, 2019.

[62] J. Chen, W. L. Jia, C. L. Yu, X. Y. Zhang, and P. A. Peng, "Bound hydrocarbons and structure of pyrobitumen rapidly formed by asphaltene cracking: implications for oil-source correlation," *Organic Geochemistry*, vol. 146, article 104053, 2020.

[63] R. C. Zheng, C. Zhao, H. N. Liu, L. Wu, R. J. Chen, and F. J. Li, "Cathodoluminescence and its significance of the Callovian-Oxfordian carbonate rocks in Amu Darya basin, Turkmenistan," *Journal of Chengdu University of Technology (Science & Technology Edition)*, vol. 37, pp. 377–385, 2010, (in Chinese with English abstract).

[64] F. J. Li, X. G. Jing, C. Y. Zou, H. Zhang, and F. Xiang, "Facies analysis of the Callovian-Oxfordian carbonates in the northeastern Amu Darya Basin, southeastern Turkmenistan," *Marine and Petroleum Geology*, vol. 88, pp. 359–380, 2017.

[65] A. M. M. Robert, J. Letouzey, M. A. Kavoosi et al., "Structural evolution of the Kopeh Dagh fold-and-thrust belt (NE Iran) and interactions with the South Caspian Sea Basin and Amu Darya Basin," *Marine and Petroleum Geology*, vol. 57, pp. 68–87, 2014.

[66] C. Y. Wu, B. S. Yu, H. J. Wang et al., "High-resolution sequence divisions and stratigraphic models of the Amu Darya right bank," *Arabian Journal of Geosciences*, vol. 12, no. 7, p. 239, 2019.

[67] H. Wang, H. Y. Fei, X. B. Cheng, and H. X. Li, "Ramp facies limestone reservoir characteristics and controlling factor of Callovian-Oxflordian in Bieshikent Depression," *Lithologic Reservoirs*, vol. 28, pp. 23–29, 2016, (in Chinese with English abstract).

[68] U. S. Geological Survey*Assessment of Undiscovered Oil and Gas Resources of the Amu Darya Basin and Afghan-Tajik Basin Provinces*US Geological Survey, Afghanistan, Iran, Tajikistan, Turkmenistan, and Uzbekistan, 2011.

[69] J. E. Neilson, N. H. Oxtoby, M. D. Simmons, I. R. Simpson, and N. K. Fortunatova, "The relationship between petroleum emplacement and carbonate reservoir quality: examples from Abu Dhabi and the Amu Darya Basin," *Marine and Petroleum Geology*, vol. 15, no. 1, pp. 57–72, 1998.

[70] J. H. Zhang, Y. Q. Liu, and L. Zhou, "Analysis of petroleum geological characteristics of the Jurassic in Karakul Block, Amu-Darya Basin," *Acta Geologica Sinica*, vol. 86, pp. 651–660, 2012, (in Chinese with English abstract).

[71] R. C. Zheng, H. N. Li, L. Wu, R. J. Chen, J. N. Shi, and F. J. Li, "Geochemical characteristics and diagenetic fluid of the Callovian-Oxfordian carbonate reservoirs in Amu Darya basin," *Acta Petrologica Sinica*, vol. 28, pp. 961–970, 2012, (in Chinese with English abstract).

[72] Y. Tian, X. Y. Zhang, G. W. Zhu et al., "Distribution characteristics of saline deposits and influences on subsalt reef-beach hydrocarbon accumulations in the right bank area of Amu Darya basin," *Science Technology and Engineering*, vol. 16, pp. 220–227, 2016, (in Chinese with English abstract).

[73] H. J. Wang, L. J. Zhang, H. L. Chen, H. W. Zhang, Z. H. Bai, and L. Z. Jiang, "Geological characteristics and distribution law of pre-salt Jurassic large and medium gas fields in the right bank of the Amu Darya River," *China Petroleum Exploration*, vol. 25, pp. 52–64, 2020, (in Chinese with English abstract).

[74] Y. Q. Guo, L. F. Liu, S. L. Zhu, and Y. X. Zhu, "Classification and assessment of petroleum system in Amu-Daria Basin," *Petroleum Exploration and Development*, vol. 33, pp. 515–520, 2006, (in Chinese with English abstract).

[75] Y. X. Yu, J. Y. Yin, J. Z. Zheng et al., "Division and resources evaluation of hydrocarbon plays in the Amu Darya Basin, Central Asia," *Petroleum Exploration and Development*, vol. 42, pp. 750–756, 2015, (in Chinese with English abstract).

[76] M. L. Nie, X. G. Tong, Q. M. Liu et al., "Types of pre-salt carbonate gas reservoirs and hydrocarbon enrichment factors of Amu Darya right bank area in Turkmenistan," *Petroleum Geology & Experiment*, vol. 38, pp. 70–75, 2016, (in Chinese with English abstract).

[77] N. X. Tian, J. Y. Yin, C. Z. Tao, and F. J. Kong, "Petroleum geology and resources assessment of major basins in Middle East and Central Asia," *Oil & Gas Geology*, vol. 38, pp. 582–591, 2017, (in Chinese with English abstract).

[78] J. C. Thomas, P. R. Cobbold, V. S. Shein, and S. Douaran, "Sedimentary record of late Paleozoic to recent tectonism in central Asia – analysis of subsurface data from the Turan and south Kazak domains," *Tectonophysics*, vol. 313, no. 3, pp. 243–263, 1999.

[79] T. Zhang, Q. Wang, and B. Liu, "Sedimentary facies and its lateral distribution of the middle-lower Jurassic in Amu Darya right bank area," *Journal of Southwest Petroleum University*, vol. 36, pp. 27–38, 2014, (in Chinese with English abstract).

[80] T. C. Guo, H. J. Wang, L. X. Mu et al., "A graphical model for halo-anhydrite components and P-wave velocity: a case study of halo-anhydrites in Amu Darya Basin," *Applied Geophysics*, vol. 13, no. 3, pp. 459–468, 2016.

[81] T. B. Coplen, "Guidelines and recommended terms for expression of stable-isotope-ratio and gas-ratio measurement results," *Rapid Communications in Mass Spectrometry*, vol. 25, no. 17, pp. 2538–2560, 2011.

[82] S. Mazur, Ł. Gągała, M. Kufrasa, and P. Krzywiec, "Application of two-dimensional gravity models as input parameters to balanced cross-sections across the margin of the East European Craton in SE Poland," *Journal of Structural Geology*, vol. 116, pp. 223–233, 2018.

[83] K. E. Peters, "Guidelines for evaluating petroleum source rock using programmed pyrolysis," *American Association of Petroleum Geologists Bulletin*, vol. 70, pp. 318–329, 1986.

[84] D. M. Jarvie, "Total organic carbon (TOC) analysis," in *Source Migration Processes and Evaluation Techniques*, R. K. Merrill, Ed., American Association of Petroleum Geologists, 1991, Treatise of Petroleum Geology Handbook of Petroleum Geology.

[85] M. Vandenbroucke and C. Largeau, "Kerogen origin, evolution and structure," *Organic Geochemistry*, vol. 38, no. 5, pp. 719–833, 2007.

[86] D. W. Waples*Geochemistry in Petroleum Exploration*International Human Resources Development Corp, Boston, 1985.

[87] M. M. El Nady, F. S. Ramadan, M. M. Hammad, and N. M. Lotfy, "Evaluation of organic matters, hydrocarbon potential and thermal maturity of source rocks based on geochemical and statistical methods: case study of source rocks in Ras

Gharib oilfield, central Gulf of Suez, Egypt," *Egyptian Journal of Petroleum*, vol. 24, no. 2, pp. 203–211, 2015.

[88] H. J. Wang, W. Wu, T. Chen, X. J. Dong, and G. X. Wang, "An improved neural network for TOC, $S_1$ and $S_2$ estimation based on conventional well logs," *Journal of Petroleum Science and Engineering*, vol. 176, pp. 664–678, 2019.

[89] B. P. Tissot andD. H. Welte*Petroleum Formation and Occurrence*Berlin, Springer Verlag, first ed. edition, 1978.

[90] Z. K. Huang, T. Liang, Z. W. Zhan, Y. R. Zou, M. W. Li, and P. A. Peng, "Chemical structure evolution of kerogen during oil generation," *Marine and Petroleum Geology*, vol. 98, pp. 422–436, 2018.

[91] B. R. T. Simoneit, "Eolian particulates from oceanic and rural areas–their lipids fulvic and humic acids and residual carbon," *Physics and Chemistry of the Earth*, vol. 12, pp. 343–352, 1980.

[92] H. L. Ten Haven, J. W. De Leeuw, and P. A. Schenck, "Organic geochemical studies of a Messinian evaporitic basin, northern Apennines (Italy) I: hydrocarbon biological markers for a hypersaline environment," *Geochimica et Cosmochimica Acta*, vol. 49, no. 10, pp. 2181–2191, 1985.

[93] M. Nishimura and E. W. Baker, "Possible origin of n-alkanes with a remarkable even-to-odd predominance in recent marine sediments," *Geochimica et Cosmochimica Acta*, vol. 50, no. 2, pp. 299–305, 1986.

[94] J. Grimalt and J. Albaigés, "Sources and occurrence of $C_{12}$-$C_{22}$ *n*-alkane distributions with even carbon-number preference in sedimentary environments," *Geochimica et Cosmochimica Acta*, vol. 51, no. 6, pp. 1379–1384, 1987.

[95] H. J. Dembicki, W. G. Meinschein, and D. E. Hattin, "Possible ecological and environmental significance of the predominance of even-carbon number $C_{20}$-$C_{30}$ *n*-alkanes," *Geochimica et Cosmochimica Acta*, vol. 40, no. 2, pp. 203–208, 1976.

[96] E. M. Galimov*Carbon Isotopes in Oil-Gas Geology*National Aeronautics and Space Administration, Washington, DC, 1973.

[97] W. J. Stahl, "Source rock-crude oil correlation by isotopic type-curves," *Geochimica et Cosmochimica Acta*, vol. 42, no. 10, pp. 1573–1577, 1978.

[98] H. M. Chung, S. W. Brand, and P. L. Grizzle, "Carbon isotope geochemistry of Paleozoic oils from Big Horn Basin," *Geochimica et Cosmochimica Acta*, vol. 45, no. 10, pp. 1803–1815, 1981.

[99] H. M. Chung, J. R. Gormly, and R. M. Squires, "Origin of gaseous hydrocarbons in subsurface environments: theoretical considerations of carbon isotope distribution," *Chemical Geology*, vol. 71, no. 1-3, pp. 97–104, 1988.

[100] C. Clayton, "Carbon isotope fractionation during natural gas generation from kerogen," *Marine and Petroleum Geology*, vol. 8, no. 2, pp. 232–240, 1991.

[101] N. Bailey, R. Burwood, and G. E. Harriman, "Application of pyrolysate carbon isotope and biomarker technology to organofacies definition and oil correlation problems in North Sea basins," *Organic Geochemistry*, vol. 16, no. 4-6, pp. 1157–1172, 1990.

[102] R. Burwood, R. J. Drozd, H. I. Halpern, and R. A. Sedivy, "Carbon isotopic variations of kerogen pyrolyzates," *Organic Geochemistry*, vol. 12, no. 2, pp. 195–205, 1988.

[103] R. Burwood, L. Jacobs, and J. Paulet, "Kerogen pyrolysis-carbon isotope technology: application to source-oil correlation problems," *Review of Palaeobotany & Palynology*, vol. 65, no. 1-4, pp. 367–377, 1990.

[104] K. E. Peters, A. E. Kontorovich, J. M. Moldowan et al., "Geochemistry of selected oils and rocks from the central portion of the West Siberian Basin, Russia," *American Association of Petroleum Geologists Bulletin*, vol. 77, pp. 863–887, 1993.

[105] W. K. Seifert and J. M. Moldowan, "Applications of steranes, terpanes and monoaromatics to the maturation, migration and source of crude oils," *Geochimica et Cosmochimica Acta*, vol. 42, no. 1, pp. 77–95, 1978.

[106] K. E. Peters, T. H. Fraser, W. Amris, B. Rustanto, and E. Hermanto, "Geochemistry of crude oils from eastern Indonesia1," *American Association of Petroleum Geologists Bulletin*, vol. 83, pp. 1927–1942, 1999.

[107] I. Rubinstein, O. Sieskind, and P. Albrecht, "Rearranged sterenes in a shale: occurrence and simulated formation," *Journal of the Chemical Society, Perkin Transactions*, vol. 19, pp. 1833–1836, 1975.

[108] D. M. McKirdy, A. K. Aldridge, and P. Ypma, "A geochemical comparison of some crude oils from pre-Ordovician carbonate rocks," in *Advances in Organic Geochemistry*, M. Bjorøy, Ed., pp. 99–107, John Wiley & Sons, New York, 1981.

[109] B. Bennett and S. D. Olsen, "The influence of source depositional conditions on the hydrocarbon and nitrogen compounds in petroleum from central Montana, USA," *Organic Geochemistry*, vol. 38, no. 6, pp. 935–956, 2007.

[110] A. Mackenzie, R. Patience, J. Maxwell, M. Vandenbroucke, and B. Durand, "Molecular parameters of maturation in the Toarcian shales, Paris Basin, France –I. Changes in the configurations of acyclic isoprenoid alkanes, steranes and triterpanes," *Geochimica et Cosmochimica Acta*, vol. 44, no. 11, pp. 1709–1721, 1980.

[111] C. C. Pan, D. H. Peng, M. Zhang, L. P. Yu, G. Y. Sheng, and J. M. Fu, "Distribution and isomerization of $C_{31}$-$C_{35}$ homohopanes and $C_{29}$ steranes in oligocene saline lacustrine sediments from Qaidam Basin, Northwest China," *Organic Geochemistry*, vol. 39, no. 6, pp. 646–657, 2008.

[112] G. Shanmugam, "Significance of Coniferous Rain Forests and related organic matter in generating commercial quantities of oil, Gippsland Basin, Australia," *American Association of Petroleum Geologists Bulletin*, vol. 69, pp. 1241–1254, 1985.

[113] J. Connan and A. M. Cassou, "Properties of gases and petroleum liquids derived from terrestrial kerogen at various maturation levels," *Geochimica et Cosmochimica Acta*, vol. 44, no. 1, pp. 1–23, 1980.

[114] R. Gratzer, A. Bechtel, R. F. Sachsenhofer, H. G. Linzer, D. Reischenbacher, and H. M. Schulz, "Oil-oil and oil-source rock correlations in the Alpine Foreland Basin of Austria: insights from biomarker and stable carbon isotope studies," *Marine and Petroleum Geology*, vol. 28, no. 6, pp. 1171–1186, 2011.

[115] H. L. Ten Haven, J. W. De Leeuw, J. Rullkotter, and J. Sinninghe Damsté, "Restricted utility of the pristane/phytane ratio as a palaeoenvironmental indicator," *Nature*, vol. 330, no. 6149, pp. 641–643, 1987.

[116] L. I. P. Dzou, R. A. Noble, and J. T. Senftle, "Maturation effects on absolute biomarker concentration in a suite of coals and associated vitrinite concentrates," *Organic Geochemistry*, vol. 23, no. 7, pp. 681–697, 1995.

[117] Y. L. Wang, X. M. Fang, T. W. Zhang et al., "Predominance of even carbon-numbered *n* -alkanes from lacustrine sediments

in Linxia Basin, NE Tibetan Plateau: Implications for climate change," *Applied Geochemistry*, vol. 25, no. 10, pp. 1478–1486, 2010.

[118] H. P. Huang, S. C. Zhang, Y. Gu, and J. Su, "Impacts of source input and secondary alteration on the extended tricyclic terpane ratio: a case study from Palaeozoic sourced oils and condensates in the Tarim Basin, NW China," *Organic Geochemistry*, vol. 112, pp. 158–169, 2017.

[119] M. I. Venkatesan, "Tetrahymanol: its widespread occurrence and geochemical significance," *Geochimica et Cosmochimica Acta*, vol. 53, no. 11, pp. 3095–3101, 1989.

[120] H. L. Ten Haven, M. Rohmer, J. Rullkötter, and P. Bisseret, "Tetrahymanol, the most likely precursor of gammacerane, occurs ubiquitously in marine sediments," *Geochimica et Cosmochimica Acta*, vol. 53, no. 11, pp. 3073–3079, 1989.

[121] A. G. Holba, W. D. Masterson, L. Ellis, and L. I. P. Dzou, "Triassic source facies in high paleo-latitude petroleum systems," in *Pacific Section AAPG/Western Region SPE Conference*, vol. 86, p. 1146, Anchorage, Alaska, 2002.

[122] A. D. Hanson, B. D. Ritts, and J. M. Moldowan, "Organic geochemistry of oil and source rock strata of the Ordos Basin, north-central China," *American Association of Petroleum Geologists Bulletin*, vol. 91, no. 9, pp. 1273–1293, 2007.

[123] A. G. Holba, L. Ellis, L. I. P. Dzou et al., "Extended tricyclic terpanes as age discriminators between Triassic, Early Jurassic and Middle-Late Jurassic oils," in *20th International Meeting on Organic Geochemistry*, p. 464, Nancy, France, 2001.

[124] J. Sepúlveda, J. Wendler, A. Leider, H. J. Kuss, R. E. Summons, and K. U. Hinrichs, "Molecular isotopic evidence of environmental and ecological changes across the Cenomanian-Turonian boundary in the Levant Platform of central Jordan," *Organic Geochemistry*, vol. 40, no. 5, pp. 553–568, 2009.

[125] P. J. Grantham, "The occurence of unusual $C_{27}$ and $C_{29}$ sterane predominances in two types of Oman crude oil," *Organic Geochemistry*, vol. 9, no. 1, pp. 1–10, 1986.

[126] A. Riboulleau, J. Schnyder, L. Riquier, V. Lefebvre, F. Baudin, and J. F. Deconinck, "Environmental change during the Early Cretaceous in the Purbeck-type Durlston Bay section (Dorset, Southern England): a biomarker approach," *Organic Geochemistry*, vol. 38, no. 11, pp. 1804–1823, 2007.

[127] P. J. Grantham and L. L. Wakefield, "Variations in the sterane carbon number distributions of marine source rock derived crude oils through geological time," *Organic Geochemistry*, vol. 12, no. 1, pp. 61–73, 1988.

[128] A. H. Knoll, R. E. Summons, J. R. Waldbauer, and J. E. Zumberge, "The Geological succession of primary producers in the oceans," in *The Evolution of Primary Producers in the Sea*, P. Falkowski and A. H. Knoll, Eds., pp. 133–163, Academic Press, Boston, 2007.

[129] F. R. A. Neto, J. M. Trendel, A. Restlé, J. Connan, and P. Albrecht, "Occurrence and formation of tricyclic terpanes in sediments and petroleums," in *Advances in Organic Geochemistry*, M. Bjorøy, P. Albrecht, C. Cornford, K. Groot, G. Eglinton, E. Galimov, D. Leythaeuser, R. Pelet, J. Rullkötter, and G. Speers, Eds., pp. 659–667, John Wiley & Sons, New York, 1983.